



Cross section measurements for neutron
induced reactions on Bi targets using
quasi mono-energetic neutron beams of
90 and 140 MeV

by

Thobeka Patience Lamula (200904141)

Dissertation submitted in partial fulfilment of the requirements for the
degree of Master of Science at the University of Zululand

Supervisors: Dr P.P Maleka

Department of Nuclear Physics, iThemba LABS

Dr S.S Ntshangase

Department of Physics, University of Zululand

Co-supervisor: Dr M.R Nchodu

Department of Nuclear Physics, iThemba LABS

September 2016

Declaration

I, the undersigned, hereby declare that the work contained in this thesis is my own original work and that I have not previously in its entirety or in part submitted it at any university for a degree.

Signature.....

Date.....

Abstract

Cross section measurements for $^{209}\text{Bi}(n,3-5n)^x\text{Bi}$ reactions were performed using quasi-monoenergetic neutron beams of 90 and 140 MeV energies. Neutron beams were produced from the $^7\text{Li}(p,n)^7\text{Be}$ reaction using the neutron beam facility of iThemba Laboratory for Accelerator Based Science (LABS). Neutron activated target materials (^{209}Bi) were analysed for gamma-ray emission with the available HPGe gamma-ray detector system of the ERL. From the identified radionuclides, their activities were determined and subsequently their production cross sections were calculated. The cross section data found from this work was compared with the existing experimental as well as the available evaluated data of the International Reactor Dosimetry Fusion File (IRDF) library. The comparison with the reported data show good agreement. Currently, other parameters are still outstanding to finalise the comparison and finally conclude the uncertainty components. The cross section data from this work will be important for testing, improving and extending the IRDF library since the existing experimental data for high energy neutrons are insufficient. To the IRDF library, the current contribution from iThemba LABS will improve the Bismuth (Bi) data for high threshold energy (n,xn) reactions with cross section peaks located at 90 and 140 MeV energies.

Acknowledgements

I would like to thank Almighty God, the creator of heaven and earth for giving me the strength, knowledge and wisdom to succeed.

To my supervisor and co-supervisor Dr Peane Maleka and Dr Rudolph Nchodu respectively, I am very thankful for guidance and support throughout the duration of this project. And for always encouraging me and giving me lot of advice throughout this study, I am very grateful to have worked with you and I hope this may continue.

I thank my supervisor, Dr Sifiso Ntshangase, for opening this opportunity of Masters studies for me and for his assistance in administration processes at the University of Zululand, for his support and words of encouragement to work hard and finish this work in time.

To Zina Ndlovu, my mentor and my big sister, I thank you for being always there when I needed your help throughout the writing up of my Masters dissertation which involves teaching me latex, my writing up was going to be hard without you. And not only that but you were also there when I needed words of encouragement, Enkosi kakhulu Zina.

I thank iThemba LABS for the beam time and the equipment used for this research work, and not forgetting to thank the people who took shifts during my experiment.

I thank all the post graduate students and friends at iThemba LABS for their support and the interactions I had with them which gave me hope and courage.

I would also like to thank the Masters in Nuclear Science lecturers, Department of Physics Administration staff at the Universities of Zululand and of the Western Cape.

I would like to thank the National Research Foundation, iThemba LABS and University of Zululand Research committee for providing funding.

To my family, my mother Bongiwe Mzolo, my father Mr Lamula and my grandmother Makhanyile Mzolo and not forgetting my uncles I thank you for allowing me to leave home and come to Cape Town to fulfil my dreams and ambitions. And I thank my best sister Sibahle Lamula for taking a good care of my daughter Senathi from day one up to this far, ngane kamama thanks alot.

To my friends and office mates Nontobeka Khumalo and Avuyile Bulala, you guys you

made each and every day to be the fun and the memorable one and you kept me inspired and you were always there to revive my hopes.

To my daughter Senathi Meloh Mashinini, thank you my princess for coming into my life and change it for the best, you are my motivation and you are the reason I wake up every morning and work hard so that you can have better future. Umama futhi uyabonga ukuthi umvumelile akushiye nogogo noncane eze kwelaseKapa ezosebenzela wena.

Ngingayikhohlwa kanjani kodwa indodakazi yami encane Uminathi Mkhwanazi, thank you my girl for coming into our family, efike nokuhle kodwa kuthina.

And last but not least I want to thank Ntokozo Mashinini for always supporting and encouraging me throughout this whole journey and for telling me that everything is going to be fine. Much love for you sthandwa sami noMelokuhle.

Dedication

- To my parents, Bongiwe Mzolo for being the best and strong mother to me and my father Mr Lamula for being supportive whenever I needed your help.
- To my grandmother, intombi yakwaKhanyile ngokusikhulisa kahle nokusinakekela njengabazukulu bakho, sibusisiwe ngokuba nogogo onothando njengawe kulomhlaba.
- To my sister Sibahle Lamula, for being my best sister and for being always there when everything seemed to be not working out and telling me that everything is going to be alright.
- To my uncles and cousins.
- And last but not least to my daughters Senathi Mashinini, Minathi Mkhwanazi and to my best half Ntokozo Mashinini.

Contents

1	Introduction	1
1.1	Motivation of the Study	1
1.2	Aims and Objectives of this Study	5
1.3	Outline of this Dissertation	6
2	Literature Review	8
2.1	Neutron Properties	8
2.1.1	Sources of Neutrons	9
2.1.2	Interactions of Neutrons with Matter	11
2.1.2.1	Neutron Cross Section	13
2.1.2.2	Neutron Flux and Fluence	15
2.1.2.3	Neutron Activation Analysis	17
2.2	Gamma Radiation	19
2.2.1	Interaction of Gamma-rays with Matter	21
2.2.1.1	Photoelectric Effect	21
2.2.1.2	Compton Scattering	22

2.2.1.3	Pair Production	23
2.3	Gamma-ray Detection	24
2.3.1	Gas-Filled Detectors	25
2.3.2	Scintillation Detectors	27
2.3.3	Semiconductor Detectors	27
3	Experimental Procedures and Equipment	29
3.1	Neutron Activation of Samples (Bi)	29
3.1.1	Target Specifications	34
3.2	Gamma-ray Spectroscopy	35
3.2.1	Energy Measurements	35
3.2.2	ERL High Purity Germanium (HPGe) Detector	36
3.2.3	Energy Calibration	40
3.2.4	Efficiency Calibration	41
3.2.5	Determination of Efficiency of the Detector.	43
4	Data Analysis, Results and Discussions	46
4.1	Identification of Radionuclides using Gamma-ray Spectroscopy	46
4.2	Determination of the Activity of radionuclides	54
4.3	Calculations of the Production Cross-section	63
4.3.1	$^{209}\text{Bi}(n,5n)^{205}\text{Bi}$ reaction	65
4.3.2	$^{209}\text{Bi}(n,4n)^{206}\text{Bi}$ reaction	67
4.3.3	$^{209}\text{Bi}(n,3n)^{207}\text{Bi}$ reaction	68

5	Conclusions and Recommendations	69
5.1	Conclusions	69
5.2	Recommendations	70

List of Figures

1.1	Experimental and Evaluated cross section data for $^{209}\text{Bi}(n,3n)^{207}\text{Bi}$ reaction.	2
1.2	Experimental and Evaluated cross section data for $^{209}\text{Bi}(n,4n)^{206}\text{Bi}$ reaction.	3
1.3	Experimental and Evaluated cross section data for $^{209}\text{Bi}(n,5n)^{205}\text{Bi}$ reaction.	3
1.4	Experimental and Evaluated cross section data for $^{209}\text{Bi}(n,6n)^{204}\text{Bi}$ reaction.	4
1.5	Experimental and Evaluated cross section data for $^{209}\text{Bi}(n,7n)^{203}\text{Bi}$ reaction.	4
1.6	Experimental and Evaluated cross section data for $^{209}\text{Bi}(n,8n)^{202}\text{Bi}$ reaction.	5
2.1	Illustration of elastic scattering	12
2.2	Illustration of fission process	13
2.3	Attenuation of an incident neutron beam of intensity (I_0) by an absorber material	14
2.4	Various reaction cross section probabilities of $^{\text{nat}}\text{Cu}$ with neutrons of energies, up to ≈ 20 MeV.	15
2.5	Neutron flux spectrum	16
2.6	Activity build-up as sample is neutron activated to t_0 (irradiation time). Counting measurements taken in the interval between t_1 and t_2	19
2.7	Illustration of the relative ability of γ , β and α radiation to penetrate different materials, such as paper, aluminium and lead.	20

2.8	Photomultiplier spectrum that shows some processes of a gamma ray interacting with matter.	22
2.9	Compton Scattering.	23
2.10	Pair production process.	24
2.11	The equivalent circuit of a gas-filled detector.	26
2.12	Gas Detector Output versus Anode Voltage.	26
2.13	Schematic diagram of a scintillation detector.	27
3.1	Separated-Sector Cyclotron Facility.	31
3.2	Schematic diagram of Neutron beam Facility.	31
3.3	(a) Neutron time-of-flight spectra obtained after irradiating a Li-target of 5 mm thickness by proton beams of 100 MeV . The two spectra were measured at neutron emission angles of 0° and at 16° respectively and they are normalized to equalize the total number of counts in the continuum region. (b) Difference spectrum obtained by subtracting the 16° spectrum from the 0° spectrum.	33
3.4	Illustration of how targets were stacked during experiment.	34
3.5	A photograph of the experimental setup showing the stacked target at (a) 0° and (b) 16°	34
3.6	Schematic diagram of electronic equipment that is used in a measurement of the energies of radiations emitted by a source.	36
3.7	Cross section diagram of HPGe detector with liquid nitrogen reservoir. . .	37
3.8	A photograph of the ERL iThemba LABS High Purity Germanium Detector. .	38
3.9	Schematic diagram of electronic setup of the ERL HPGe detector system. .	39
3.10	Energy Calibration plot obtained using Th-234 source.	40

3.11	Gamma ray spectrum of ^{152}Eu point source.	41
3.12	Gamma ray spectrum of ^{60}Co point source.	42
3.13	Gamma ray spectrum of ^{137}Cs point source.	42
3.14	Efficiency of the detector for each gamma-ray energy of the sources (^{152}Eu , ^{60}Co and ^{137}Cs).	45
4.1	Level scheme of the decay of ^{207}Bi	47
4.2	Full gamma ray spectrum of $^{209}\text{Bi}(\text{n},\text{xn})$ reaction where neutron beam of 90 MeV energy was used.	48
4.3	Selected region (500 - 600 keV) for $^{209}\text{Bi}(\text{n},\text{xn})$ reaction spectrum showing the identified 511 keV annihilation peak and the identified ^{205}Bi , ^{206}Bi and ^{207}Bi radionuclides.	49
4.4	Selected region (680 - 720 keV) showing $^{209}\text{Bi}(\text{n},5\text{n})^{205}\text{Bi}$ reaction 703.5 keV photopeak.	50
4.5	Selected region (790 - 820 keV) showing $^{209}\text{Bi}(\text{n},4\text{n})^{206}\text{Bi}$ 802.9 keV reaction photopeak.	50
4.6	Full gamma ray spectrum of $^{209}\text{Bi}(\text{n},\text{xn})$ reaction where neutron beam of 140 MeV energy was used.	51
4.7	Selected region (500 - 580 keV) showing $^{209}\text{Bi}(\text{n},3\text{n})^{207}\text{Bi}$ reaction photopeak and 511 keV annihilation peak.	52
4.8	Selected region (680 - 740 keV) showing $^{209}\text{Bi}(\text{n},5\text{n})^{205}\text{Bi}$ reaction 703.4 keV photopeak.	53
4.9	Selected region (760 - 820 keV) showing $^{209}\text{Bi}(\text{n},4\text{n})^{206}\text{Bi}$ reaction 802.9 keV photopeak.	53
4.10	The activity (Bq) of ^{205}Bi radionuclide as a function of energy for the reac- tion of $^{209}\text{Bi}(\text{n},5\text{n})$ at neutron beam energy of 90 MeV.	56

4.11	The activity (Bq) of ^{206}Bi radionuclide as a function of energy for the reaction of $^{209}\text{Bi}(n,4n)$ at neutron beam energy of 90 MeV.	57
4.12	The activity (Bq) of ^{207}Bi radionuclide as a function of energy for the reaction of $^{209}\text{Bi}(n,3n)$ at neutron beam energy of 90 MeV.	58
4.13	The activity (Bq) of ^{205}Bi radionuclide as a function of energy for the reaction of $^{209}\text{Bi}(n,5n)$ at neutron beam energy of 140 MeV.	60
4.14	The activity (Bq) of ^{206}Bi radionuclide as a function of energy for the reaction of $^{209}\text{Bi}(n,4n)$ at neutron beam energy of 140 MeV.	61
4.15	The activity (Bq) of ^{207}Bi radionuclide as a function of energy for the reaction of $^{209}\text{Bi}(n,3n)$ at neutron beam energy of 140 MeV.	62
4.16	The neutron induced cross sections of $^{209}\text{Bi}(n,5n)^{205}\text{Bi}$ reaction from the present work (Lamula-2016) compared with the results of earlier measurements and model calculations.	66
4.17	The neutron induced cross sections of $^{209}\text{Bi}(n,4n)^{206}\text{Bi}$ reaction from the present work (Lamula-2016) compared with the results of earlier measurements and model calculations.	67
4.18	The neutron induced cross sections of $^{209}\text{Bi}(n,3n)^{207}\text{Bi}$ reaction from the present work (Lamula-2016) compared with the results of earlier measurements and model calculations.	68

List of Tables

2.1	Typical classification of neutrons.	9
3.1	Table that shows the activated discs (labelled: Bi_1, Bi_2, Bi_3 and Bi_4) after the irradiation experiment.	35
3.2	Determination of the detector efficiency using (^{152}Eu , ^{60}Co and ^{137}Cs) certified reference point sources.	44
4.1	Activity and weighted average activity of radionuclides produced from ^{209}Bi that was irradiated with 90 MeV neutron beam.	55
4.2	Activity and weighted average activity of radionuclides produced from ^{209}Bi that was irradiated with 140 MeV neutron beam.	59
4.3	Table that shows the cross section result of neutron induced reactions.	64
4.4	Table shows the components that contribute to the uncertainty of the production cross section of radionuclides.	65

Chapter 1

Introduction

Nuclear data as quantitative characteristics of nuclear reactions have become important in the intermediate energy range. They are important for the development of new concepts of nuclear energy production and changing of radioactive waste with the use of accelerators as well as for design of shielding for accelerators, medical therapies and many other applications. They are also important for the development of theory of nuclear interactions, nuclear structure and nuclear matter properties [1]. The goal of the nuclear data community is to produce high quality nuclear data libraries for existing and future nuclear energy systems [2]. This study focuses on determining the experimental neutron cross section data on a ^{209}Bi target that will be included in the IRDFF (International Reactor Dosimetry and Fusion File) library.

1.1 Motivation of the Study

Measurements of cross sections for the (n,3-8n) reactions on a Bi target using quasi mono-energetic neutron beams of 40 to 200 MeV were proposed at iThemba LABS for the IRDFF library. The IRDFF library consists of more than 70 reactions that are important for reactor dosimetry, fusion and fission studies. At the IAEA (International Atomic Energy Agency) Consultants Meeting to Review the Requirements to Improve and Extend the IRDFF library (i.e. IRDF-2002), it was indicated that the available experimental data for these dosimetry reactions are insufficient, in particular at higher neutron energies, i.e.

above the 20 MeV threshold [3].

The few existing experimental data have large uncertainties (30-50%) and there is disagreement between measured data and theoretical model predictions at energies above 30 MeV [3]. Theoretical model calculations provide an additional source of cross-section data but more experimental data are still required for benchmarking calculations and for the adjustment of model parameters. New evaluations are proposed on the basis of new experimental data combined with data obtained from consistent theoretical model calculations. Existing circumstances are demonstrated for reactions ($^{209}\text{Bi}(n,3n)^{207}\text{Bi}$) for neutron energies above 20 MeV refer to Figures 1.1 to 1.6, respectively [4]. The experimental data are not sufficient due to the limited number of facilities available to provide high energy neutrons ($E_n = 40$ MeV). Measurements of neutron-induced cross sections were previously performed at iThemba LABS at energy range of 40 to 150 MeV [5, 6].

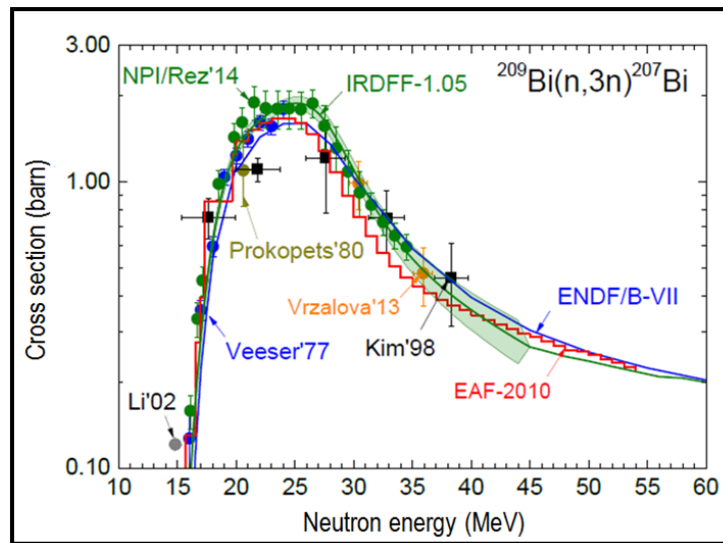


Figure 1.1. Experimental and Evaluated cross section data for $^{209}\text{Bi}(n,3n)^{207}\text{Bi}$ reaction [4].

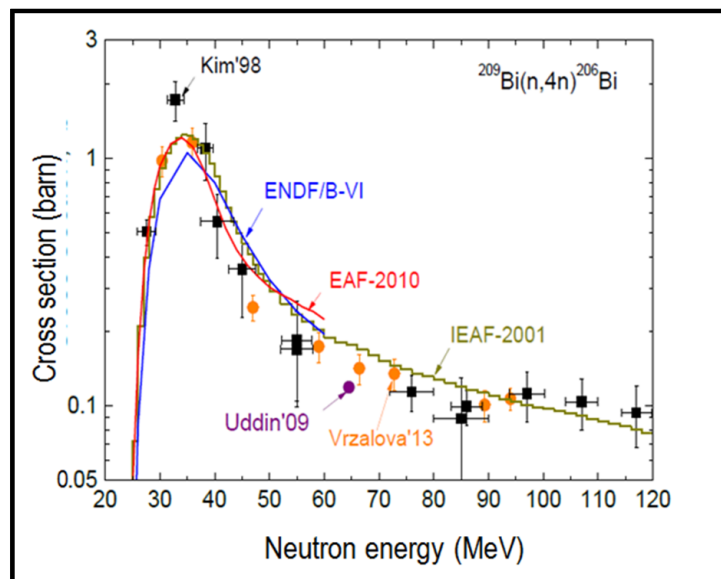


Figure 1.2. Experimental and Evaluated cross section data for $^{209}\text{Bi}(n,4n)^{206}\text{Bi}$ reaction [4].

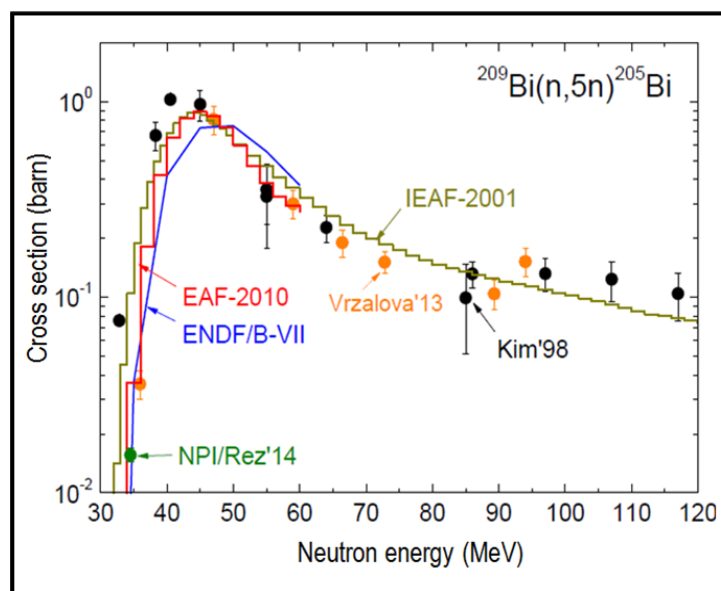


Figure 1.3. Experimental and Evaluated cross section data for $^{209}\text{Bi}(n,5n)^{205}\text{Bi}$ reaction [4].

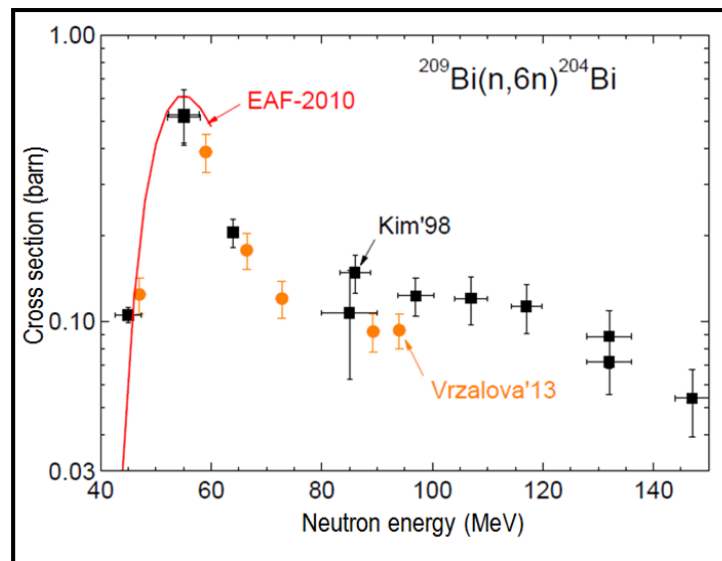


Figure 1.4. Experimental and Evaluated cross section data for $^{209}\text{Bi}(n,6n)^{204}\text{Bi}$ reaction [4].

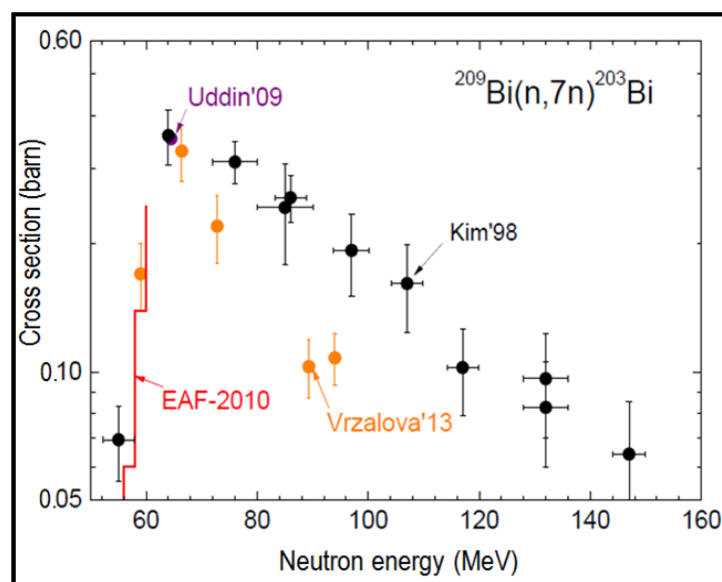


Figure 1.5. Experimental and Evaluated cross section data for $^{209}\text{Bi}(n,7n)^{203}\text{Bi}$ reaction [4].

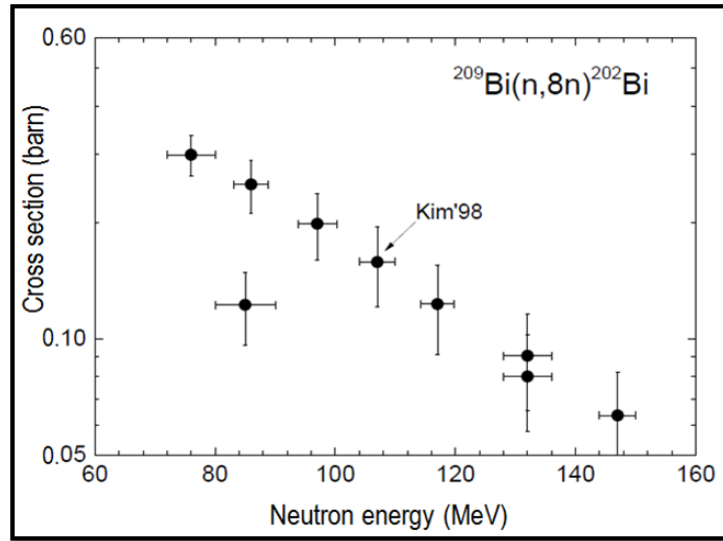


Figure 1.6. Experimental and Evaluated cross section data for $^{209}\text{Bi}(n,8n)^{202}\text{Bi}$ reaction [4].

1.2 Aims and Objectives of this Study

A set of (n,3-8n) reactions on ^{209}Bi are important for neutron fluence monitoring and spectra unfolding at the high energy accelerator driven neutron sources. Furthermore these data will be important for validation of energy extension by quasi-monoenergetic sources for testing and improving the IRDFF library. The IRDFF library is an evaluated cross section library of neutron dosimetry reactions. This library can be used in a range of applications from assessments of nuclear power reactors and other neutron metrology applications such as Boron neutron capture therapy, therapeutic use of medical isotopes, nuclear physics measurements, and reactor safety applications.

The high energy neutrons have increasingly been used for nuclear physics, solid state physics, radiotherapy and so on. This increases the demand for neutron cross sections in the high energy region. Safety design consideration for the accelerator facilities requires activation and spallation cross sections for high energy neutrons to estimate the radioactivities induced in the accelerator components and in the shielding materials. The study of neutron cross sections is also important for the development of fission reactor technology from the point of activation, radiation damages and radiation protection. In addition, this study aims to provide additional experimental data for the neutron induced reactions

($^{209}\text{Bi}(n,3-8n)$) at high energies ($E_n = 90$ and 140 MeV) and thus also improve on the uncertainties.

1.3 Outline of this Dissertation

This present study is about cross section measurements for neutron induced reactions on a ^{209}Bi target using quasi-monoenergetic neutron beams of 90 and 140 MeV energy.

Chapter 1 provides background information concerning this work which includes the existing measurements which was previously reported and a plan to improve the existing experimental cross section data, which lead to the motivation and the aim of this study.

Chapter 2 gives a review of relevant theory on which this study is based. Since neutrons were used to irradiate samples, neutrons as well as their sources and properties, which includes their interaction with matter and their cross sections are discussed here. This is followed by the theory related to gamma-rays, as the secondary particles that are measured from radioactive samples after the activation of sample with neutrons. In this chapter gamma ray interaction with matter and gamma ray detection are also discussed.

Chapter 3 covers the experimental procedure and equipments used in this study. Additionally, the neutron activation of a sample (^{209}Bi target) using the neutron beam facility of iThemba LABS. This is followed by gamma ray spectroscopy which gives more details about gamma ray energy measurements and the HPGe detector used in this study, and subsequently to data acquisition and electronics used in collecting data. Energy and efficiency calibration of the gamma-ray detector is discussed in this chapter.

Chapter 4 presents the data analysis and results, which demonstrates steps that were used and followed in the process of determining the neutron cross sections. This involves gamma ray measurements using the HPGe detector and the gamma ray spectra analysis for a purpose of identifying the radionuclides produced after irradiating ^{209}Bi target with neutron beams. The activity was then used to determine the cross section of each neutron induced reaction.

Chapter 5 discusses the conclusions and recommendations of this study, which covers the findings of cross section measurements and also discusses the comparison of new data from

this study with existing evaluated and experimental data.

Chapter 2

Literature Review

In this chapter, the theory related to this study is discussed. The neutron production theory is provided where the explanation of different sources of neutrons are given as well as types of neutron cross sections and reaction rates. For this study neutrons were produced using a nuclear reaction process, where a proton beam was used to bombard a Li target. Gamma radiation is also discussed where the processes of gamma ray interaction with matter and different types of gamma ray detectors are clearly explained. For this work a semiconductor detector (High Purity Germanium (HPGe) detector) was used for gamma ray measurement.

2.1 Neutron Properties

The first experimental observation of the neutron took place in 1930 when Bothe and Becker fired beryllium with an alpha particle from a radioactive decay and found a very penetrating but non-ionizing radiation [7]. They assumed it was a gamma-ray of high energy, and later Curie and Joliot observed that when this radiation fell on paraffin, an energetic (5.3 MeV) proton was emitted [7]. And they computed that if this radiation is indeed of gamma-rays its energy would be 52 MeV to release such protons, and the energy of the emitted gamma-rays seemed to be completely unlikely. Chadwick later in 1932 came up with the correct explanation of identifying the unknown radiation as neutral (penetrating and non-ionizing) particle with mass nearly the same as that of a proton [7].

The neutron is a neutral particle which is stable inside the nucleus of an atom, outside the nucleus it decays (beta-decays) with a mean lifetime of about 15 min. The rest mass of a neutron is equivalent to 1.67482×10^{-27} kg (1 atomic mass unit) [8]. Since a neutron carry no charge it plays a fundamental role in study of nuclear forces. Unaffected by coulomb barrier, neutrons of even very low energies (eV or even less) can penetrate the nucleus and start up nuclear reactions [7]. Neutrons can travel through very thick matter without any kind of interaction. When in any case a neutron undergoes the interaction, it is with the nucleus present in the absorbing material. As a result of the interaction the neutron may either disappear and be replaced by one or more secondary radiations, or else there is a change of energy or direction of a neutron [9].

2.1.1 Sources of Neutrons

Neutrons produced are classified based on their kinetic energies as shown in Table 2.1 [10].

Table 2.1. Typical classification of neutrons.

Energy (E_n)	Class
$E_n \approx 0.025$ eV	Thermal neutrons
$E_n < 0.5$ eV	Slow neutrons
0.025 eV $\leq E_n \leq 0.5$ MeV	Epithermal neutrons
$E_n > 0.5$ MeV	Fast neutrons

Thermal neutrons are neutrons in thermal equilibrium with the atoms of the moderator and they are characterised by very low energies. At room temperatures (293 K), their energy spectrum is best described by a Maxwell distribution with the maximum value corresponding to the neutron kinetic energy $E = \frac{3}{2}kT$ (where k is the Boltzmann constant, and T is the room temperature in Kelvin) [?]. At room temperature, the energy spectrum of thermal neutrons is best described by a Maxwell-Boltzmann distribution with a mean energy of 0.025 eV and a most probable velocity of 2200 m.s⁻¹ [11]. The most probable neutron velocity can be calculated using Equation (2.1).

$$v_{mp} = \sqrt{\frac{2kT}{m}} \quad (2.1)$$

where: k = Boltzmann constant (1.38×10^{-23} J/K)

T = temperature in Kelvin and

m = neutron mass (1.66×10^{-27} kg).

$$v_{mp} = \sqrt{\frac{2(1.38 \times 10^{-23})(293)}{1.66 \times 10^{-27}} \left(\frac{kg \cdot m^2 \cdot s^{-2}}{kg} \right)} = 2200 m \cdot s^{-1} \quad (2.2)$$

Epithermal neutrons are the neutrons which are in the process of slowing down by colliding with nuclei of the moderator. A Cd foil of 1 mm thickness in a reactor cuts off all thermal neutrons but allows epithermal and fast neutrons, with energies greater than 0.5 eV, to pass through. Due to its large absorption cross section for thermal neutrons, Cd absorbs thermal neutrons strongly. Typically the epithermal neutron flux represents about 2% of the total reactor neutron flux [11].

Fast neutrons are neutrons with energy greater than 0.5 MeV and can induce nuclear reactions where the ejection of one or more nuclear particles - (n,p), (n,n') and (n,2n) are likely. Typically, about 5% of the total reactor neutron flux consists of fast neutrons [11]. Neutron beams can be produced from various sources, and since neutrons are neutral particles (not charged) they can not be accelerated [7]. Some of the options available for neutron sources/production are discussed below.

1. The alpha-Beryllium Source: Many targets material may lead to (α ,n) reactions for the alpha particle energies that are available in radioactive decay. Choosing beryllium as the target produces maximum neutron flux. As shown in Equation (2.3), a Be-target is bombarded by α particle to produce neutron and stable carbon nucleus [9].



2. Neutron-induced fission: Is a source of neutrons where neutrons are produced from nuclear fission processes. Nuclear fission process is a nuclear reaction where heavy nucleus splits into two or more smaller nuclei and neutrons of high energies are produced. As shown in Equation (2.4), uranium is irradiated with thermal neutrons and an unstable uranium is produced, it then splits into two nuclei (strontium and xenon) and neutrons are emitted [8].



3. Nuclear reactions: These reactions require the accelerator to produce a particle beam to initiate the reaction, by selecting the energy of a beam and the angle at which the neutron emitted is observed, mono-energetic neutron beam is produced. The reaction in Equation (2.5) illustrates this process.



2.1.2 Interactions of Neutrons with Matter

Since neutrons are uncharged, their interaction with electrons in a matter proceeds via the magnetic moments of the two particles rather than the coulomb force. The neutrons interact with the nuclei of an atom through a strong nuclear interaction. This hadronic interaction has a very short range, thus the neutron have to pass very close to the nucleus to occur [12].

When a neutron collides with the atom nuclei, it may lead to various scenarios, such as, elastic scattering, inelastic scattering, transmutation and fission [10].

Elastic scattering (n,n) occurs when a neutron strikes a nucleus and rebounds elastically. In such a collision the total kinetic energy and momentum are conserved. Figure 2.1 illustrates an elastic scattering of a neutron. The neutron loses energy that is gained by the target nucleus which moves away. And if the target nucleus is light, neutron loses much energy (very effective slowing down process). This process is not effective in slowing down neutrons with very high energy (above 150 MeV).

Inelastic scattering (n,n'γ) occurs when a neutron strikes and enters a nucleus. In this collision the total kinetic energy is not conserved, while the total momentum is conserved

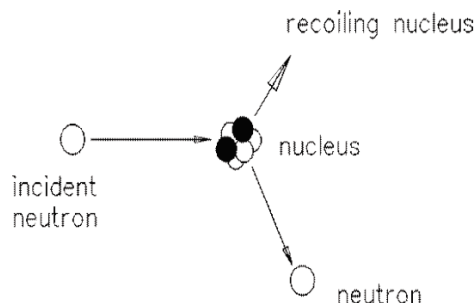
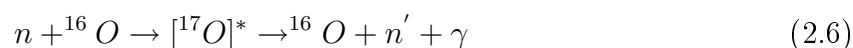


Figure 2.1. Illustration of elastic scattering [10].

[13]. Equation (2.6) shows the process of inelastic scattering. When a neutron strikes a nucleus (^{16}O) it forms an unstable compound nucleus (^{17}O) which emits neutron (n') and a gamma-ray (γ) thus returning back to the target nucleus (^{16}O).



The capture of neutrons may lead to the formation of new nuclei (transmutation), or may lead to the fragmentation of the nucleus (fission) or the emission of other nuclear particles from the nucleus.

Transmutation (n,p) or (n, α) occurs when a nucleus absorbs neutrons and forms an excited compound nucleus which de-excites by emitting charged particle either a proton or an alpha particle, one result could initiate a sequence of events and that could lead to the formation of new nuclide. Equation (2.7) shows an example of transmutation (n,p) reaction, where oxygen (^{16}O) absorbs a neutron and forms an excited compound nucleus (^{17}O) and emits a proton (^1H) to form nitrogen (^{16}N).



Radiation capture reaction (n, γ) is nuclear reaction in which a target nucleus absorbs a neutron, then emits a discrete quantity of electromagnetic energy (γ -ray). See Equation (2.8) where hydrogen (^1H) nucleus absorbs a neutron to produce deuterium (^2H) [14].



Nuclear fission is a process whereby an incident neutron enters a heavy target nucleus (e.g. ${}^{235}\text{U}$ and ${}^{239}\text{Pu}$), causing the nucleus to "split" (fission) into two or more large fragments, during which energy and further neutrons are released. Nuclear fission reactors are mostly based on the induced fission reactions of ${}^{235}\text{U}$ and ${}^{239}\text{Pu}$ to yield 2 to 3 neutrons per fission at kinetic energies of approximately 2 MeV [15] [9]. The example of a fission process is shown in Figure 2.2 [16] and a typical fission reaction of uranium (${}^{235}\text{U}$) and neutron is given in Equation (2.4).

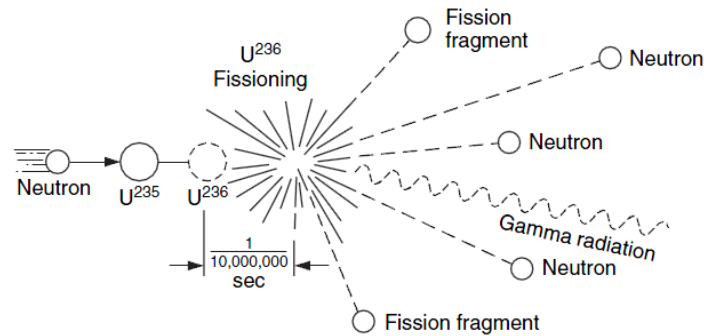


Figure 2.2. Illustration of fission process [16].

2.1.2.1 Neutron Cross Section

Neutron cross section is a probability at which a particular material will interact with a neutron of given energy. To understand the concept of cross section one may consider a simple case shown in Figure 2.3 with neutron beams entering a material of unit area (in cm^2) and thickness x (in cm).

The intensity of neutrons passing through the material decreases depending on the number of nuclei per unit volume of the material (N) in cm^{-3} and the effective area of obstruction (in cm^2) presented by a single nucleus. This area of obstruction is called microscopic cross section (σ) of the material. The microscopic cross section is an area measured in barns (b), where a barn is equivalent to 10^{-24} cm^2 .

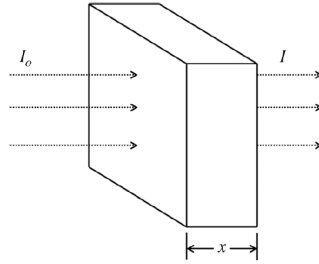


Figure 2.3. Attenuation of an incident neutron beam of intensity (I_0) by an absorber material [10].

Equation (2.9) is specific for only one type of reaction when the absorber material contains only one type of pure nuclide.

$$I = I_0 \cdot e^{-N\sigma x} \quad (2.9)$$

where the quantity ($N\sigma$) is called the macroscopic cross section or obstruction coefficient (Σ) (in cm^{-1}) [10]. And N , the number of nuclei per unit volume of material is given by Equation (2.10):

$$N = \frac{\rho \cdot N_A}{M} \quad (2.10)$$

where ρ is density ($\text{g}\cdot\text{cm}^{-3}$), N_A is Avogadro's number (per mol) and M is atomic weight (g/mol).

Macroscopic cross section is the number of reactions (e.g. scattering, absorption, fission, etc.) which a neutron undergoes per unit distance of travel. The nuclear cross sections for scattering (Σ_s), absorption (Σ_a) and fission (Σ_f) depend on the material in which the neutron is travelling and are typically functions of the energy of the neutron. The total cross section Σ_{tot} which is a measure of total number of all types of reaction per unit distance, may be seen in equation (2.11) [10].

$$\Sigma_{tot} = \Sigma_s + \Sigma_a + \Sigma_f + \dots \quad (2.11)$$

A feature that describes the transmission of neutrons through matter is called mean free path length. It is the mean distance a neutron travels between interactions. It can be calculated from equation (2.12) and is a reciprocal of the macroscopic cross section.

$$\lambda = \frac{1}{\Sigma_{tot}} \quad (2.12)$$

Figure 2.4 shows the reaction cross section plot, which are the reactions possible if natural copper (^{nat}Cu) interact with a neutron. Those reactions are elastic, inelastic scattering and total cross section.

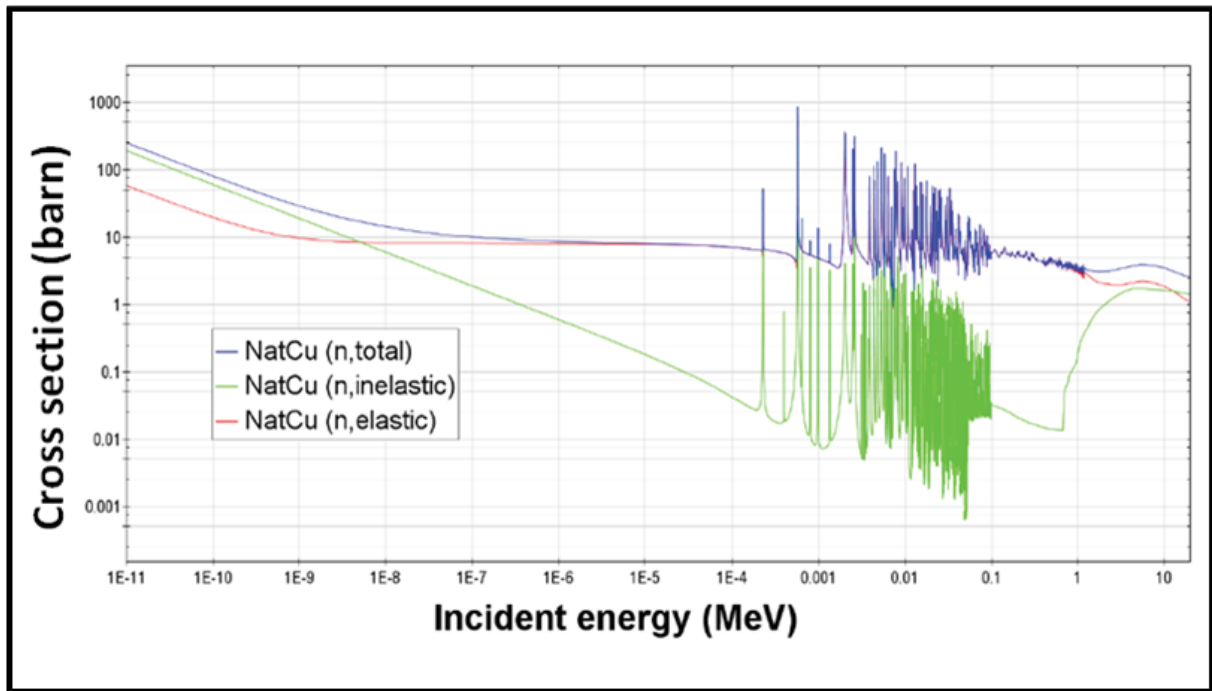


Figure 2.4. Various reaction cross section probabilities of ^{nat}Cu with neutrons of energies, up to ≈ 20 MeV [17].

2.1.2.2 Neutron Flux and Fluence

The neutron flux (neutrons per cm^2 per second) is defined as the product of the neutron density (n) which is number of neutrons per unit volume and the velocity (v), expression of determining neutron flux (ϕ) is shown in Equation (2.13) [18].

$$\phi(v) = nv \quad (2.13)$$

Neutron flux is equal to the total distance (sum of all the path lengths) travelled in one second by all the neutrons present in one cm^3 . This Equation (2.13) is for monoenergetic neutrons. Figure 2.5 shows a typical neutron flux spectrum of a reactor. From the spectrum

it is clear that thermal neutrons always have the highest flux, whereas flux of epithermal and fast neutrons mainly depend on the type of the moderator used [19].

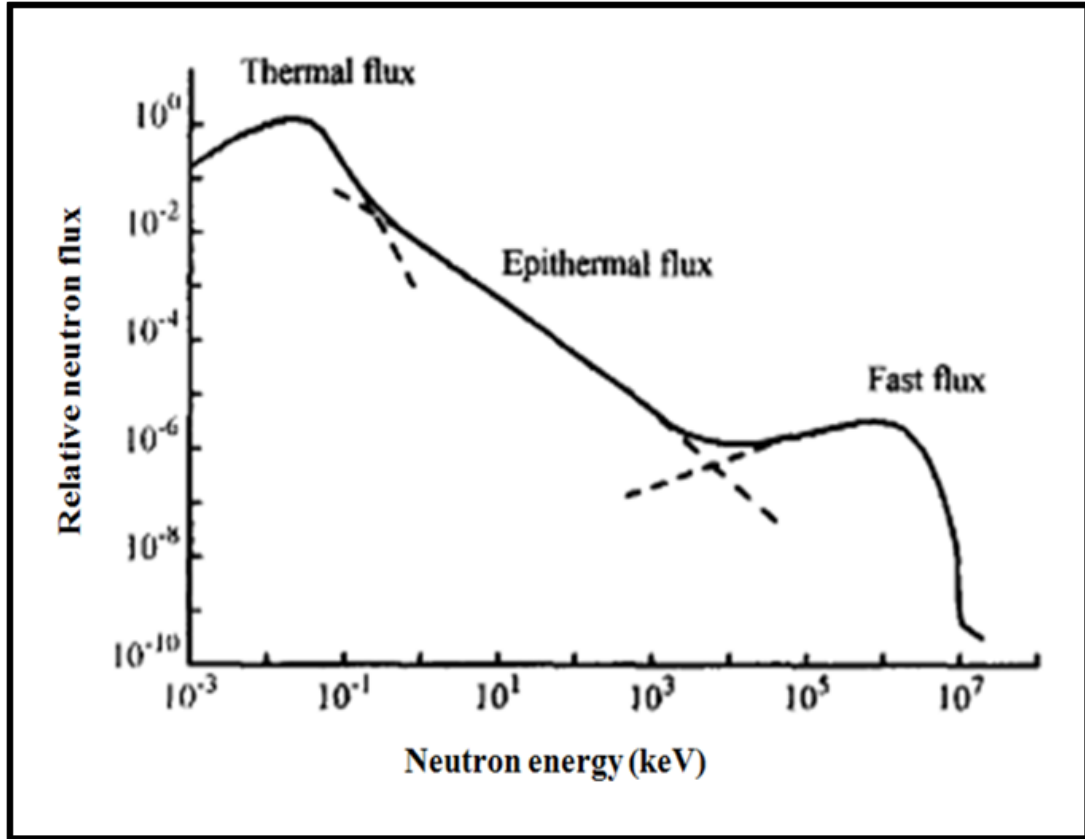


Figure 2.5. Neutron flux spectrum [20].

In case of a distribution of velocities v , the total flux is obtained by integrating over velocity as shown in Equation (2.14).

$$\phi = \int n(v)v dv \quad (2.14)$$

The reaction rate (R) which is a probability of a neutron to interact with the material can be expressed as a function of the neutron flux in the equation (2.15). This Equation (2.15) is for (quasi-monoenergetic neutrons) [18].

$$R = \Sigma v \phi(v) \quad (2.15)$$

If there is a distribution of neutron velocities, the reaction rate can be integrated over the

distribution as shown in Equation (2.16), i.e., reaction rate over all neutrons

$$R = \int \Sigma v \phi(v) dv \quad (2.16)$$

2.1.2.3 Neutron Activation Analysis

Neutron Activation Analysis (NAA) is a technique where sample is irradiated by neutron beams to induce radioactivity. After J. Chadwick discovered a neutron in 1932 and the results of F. Joliot and I. Curie in 1934, the neutron activation analysis was first developed by G. Hevesy and H. Levi in 1936.

They used a ($^{226}\text{Ra} + \text{Be}$) neutron source and a radiation detector (ionization chamber). They discovered that the element Dy (dysprosium) in the sample became highly radioactive and unstable after being exposed to the neutron source. They observed that the nuclear reaction can be used to determine the elements present in unknown samples by measuring the induced radioactivity [21].

Consider a target material irradiated by neutron beams such that neutron capture process occurs. The target will either remain stable or become more unstable. In the latter case, the nuclei will become unstable or excited and undergo β -decay by emitting γ -rays which can be detected using a High Purity Germanium (HPGe) detector [22]. The net rate of the radioactive nuclei is governed by the expression in Equation (2.17).

$$\frac{dN(t)}{dt} = -\lambda N(t) + P(t) \quad (2.17)$$

Where $N(t)$ is the number of radioactive nuclei, λ is the decay constant in s^{-1} and is given by the expression: $\lambda = \frac{1}{\tau}$, where τ is mean life and $P(t)$ is the production rate which is represented by Equation 2.18.

$$P(t) = N_0 \sigma \phi(t) \quad (2.18)$$

Where N_0 is the number of target nuclei, σ is the cross section ($\text{barn} = 10^{-24} \text{ cm}^2$), $\phi(t)$ is the neutron flux.

Substituting equation (2.18) in Equation (2.17) then Equation (2.17) becomes;

$$\frac{dN(t)}{dt} = -\lambda N(t) + N_0 \sigma \phi(t) \quad (2.19)$$

The general solution for $N(t)$ for a constant flux is expressed as follows:

$$N(t) = \frac{N_0\sigma\phi}{\lambda}(1 - e^{-\lambda t}) \quad (2.20)$$

From radioactive decay, the activity is the rate of change of number of radioactive nuclei $N(t)$ per time t ,

$$A(t) = -\frac{dN(t)}{dt} = \frac{1}{\tau}N(t) = \lambda N(t) \quad (2.21)$$

Equation (2.21) can be written as Equation (2.22).

$$A(t) = \lambda N(t) = N_0\sigma\phi(1 - e^{-\lambda t}) \quad (2.22)$$

Considering an irradiation time (t_{irr}) then the activity $A(t_{irr})$ during irradiation becomes;

$$A(t_{irr}) = N_0\sigma\phi(1 - e^{-\lambda t_{irr}}) \quad (2.23)$$

The activity $A(t_{irr}, t_d, t_c)$ of a radionuclide at the start of the gamma ray measurement is given by Equation (2.24).

$$A(t_{irr}, t_d, t_c) = N_0\sigma\phi(1 - e^{-\lambda t_{irr}})e^{-\lambda t_d} \quad (2.24)$$

The irradiated sample may not be measured using HPGe detector immediately after irradiation, therefore counting interval from t_d to t_c have to be taken into consideration, where t_d represents the delayed time and t_c is the gamma ray spectra counting time.

The activity during measurement is given by Equation (2.25);

$$A(t_{irr}, t_d, t_c) = N_0\sigma\phi(1 - e^{-\lambda t_{irr}})e^{-\lambda t_d}(1 - e^{-\lambda t_c}) \quad (2.25)$$

Figure 2.6 shows the behaviour of a sample irradiated with neutron beam. During activation there is a build-up in activity. After a long time the induced activity will gradually reach equilibrium state, which is known as saturation such that the production rate and destruction rate are equal.

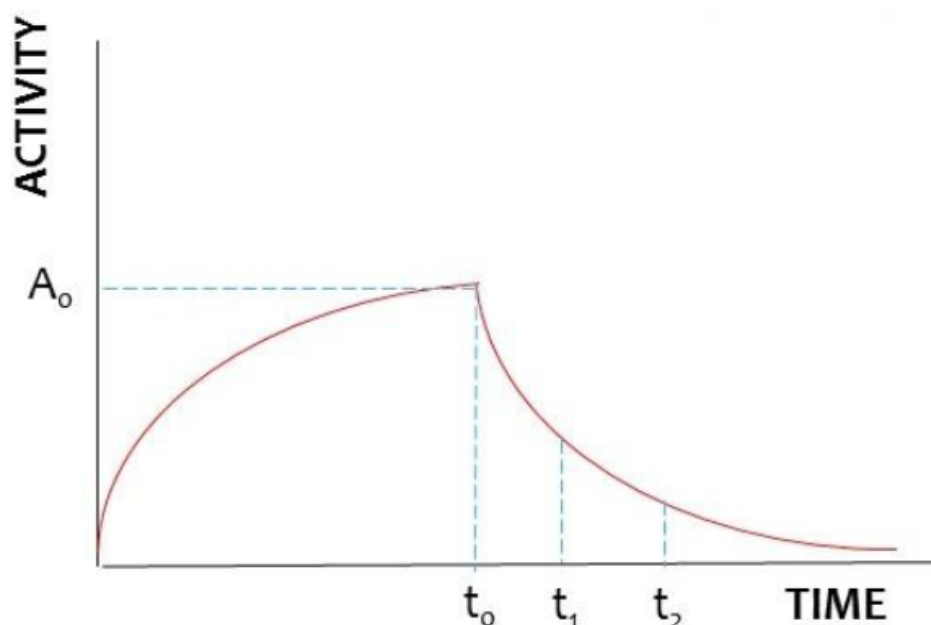


Figure 2.6. Activity build-up as sample is neutron activated to t_0 (irradiation time). Counting measurements taken in the interval of t_1 and t_2 . [22].

2.2 Gamma Radiation

Wilhelm Conrad Rontgen's sensational discovery of X-rays in 1895 was soon followed by Henri Becquerel's discovery of radioactivity and by J. J. Thomson's proof of the independent existence of negative electrons of small mass. Marie and Pierre Curie discovered the radioactive elements polonium and radium, and Paul Villard observed a new kind of extremely penetrating ray, later called gamma rays [23].

Paul Villard's main interest was in chemistry studies, which led him into his studies of "radium rays", X-rays and cathode rays. His radioactivity experiments resulted in the unexpected discovery of gamma rays in 1900. Villard observed gamma rays as being different from X-rays because they showed bigger penetrating depth. He also discovered that they were emitted from substances that are radioactive and were not affected by magnetic and electric fields. Even though Paul Villard had discovered gamma rays, Ernest Rutherford recognised that they were in the form of electromagnetic (EM) light only with shorter wavelength than X-rays. The name gamma ray was given by Ernest Rutherford [24].

Gamma radiation which is also called gamma rays is an electromagnetic radiation (of high frequency and therefore consists of high energy photon) that is emitted by an unstable nucleus of an atom during radioactive decay. A nucleus which is in an unstable state may decay to a more stable state or ground state by the emission of energy as gamma radiation [8].

There are many other radioactive decays such as beta (β) and alpha (α) decays. Beta decay is when a nucleus with either too many protons or too many neutrons undergo β decay through the weak nuclear force, a neutron-rich nucleus will undergo β^- emission ($n \rightarrow p^+ + e^- + \bar{\nu}$) and a proton-rich nucleus will either emit a β^+ particle ($p \rightarrow n + e^+ + \nu$) or be transformed by capturing an atomic electron in a process called electron capture.

Alpha decay is the radioactive emission of an α particle which is the nucleus of ^4He , consisting of two protons and two neutrons.

Beta (β) particles have a negative charge and a small mass. Unlike γ ray they have very low energies and may be shielded by the aluminium material while alpha (α) particles are positively charged and are also not very penetrating. Gamma (γ) rays are the most penetrating particles since they are not charged and have a very short wavelength and high energy.

Figure 2.7 shows the ability of different types of ionizing radiation to penetrate different materials [25]. This study focuses more on detection of gamma rays and using their energies to identify the radionuclides produced from the nuclear reactions.

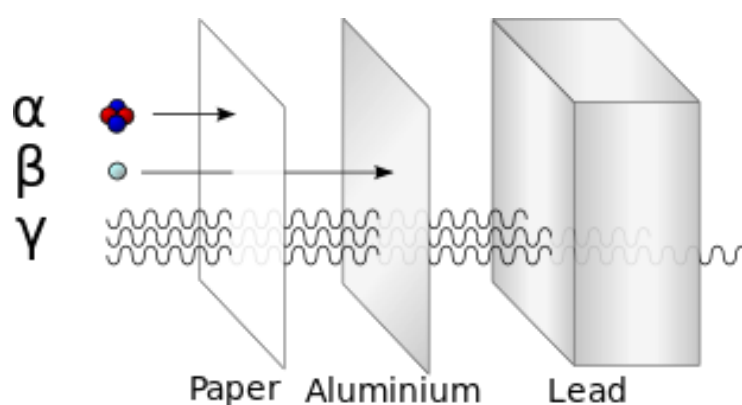


Figure 2.7. Illustration of the relative ability of γ , β and α radiation to penetrate different materials, such as paper, aluminium and lead [25].

2.2.1 Interaction of Gamma-rays with Matter

Like neutrons, gamma rays have no mass and no charge and so they need an indirect way to transfer energy. Unlike charged particles (electrons and protons), the penetrating power of gamma rays is very high [26, 27]. The interaction of gamma radiation with matter causes ionization in matter via three major processes. These three processes are the photoelectric effect, Compton scattering and pair production. The mass attenuation coefficient (μ_m) defined in Equation (2.26) is a measure of the probability of a γ ray interacting in the material.

$$\mu_m = \frac{\mu}{\rho} \quad (2.26)$$

Where ($\mu = N\sigma$) is the linear attenuation coefficient, σ is the total interaction cross section per atom of material and ρ is the physical density. It depends on the atomic number, Z of the atom of the absorbing material, and it varies with the γ ray energy (E_γ) and has contributions from all the three γ ray interaction processes that occur in the absorbing material [26]. The gamma ray interaction processes with matter are discussed in the next subsection.

2.2.1.1 Photoelectric Effect

In photoelectric absorption process, a photon undergoes an interaction with an absorber atom in which a photon completely disappears. In its place an energetic photoelectron is released by the atom from one of its outer most shells [9]. Since the energy of the gamma ray (≈ 0.5 MeV) is greater than the electron binding energy (which is about 10 to 100 eV), the energy of the free electron can be considered equal to that of the incident gamma ray. Therefore the photoelectric effect results in a peak known as photopeak in the photomultiplier spectrum at an energy same as the energy of an incident gamma ray. Figure 2.8 shows a photomultiplier spectrum [28].

Energy of the photoelectron is given by:

$$E_e = hv - E_b \quad (2.27)$$

where (E_b) is the photoelectron binding energy in its original shell. Binding energy is the energy required to remove an electron from an atom or a molecule and hv is the energy of

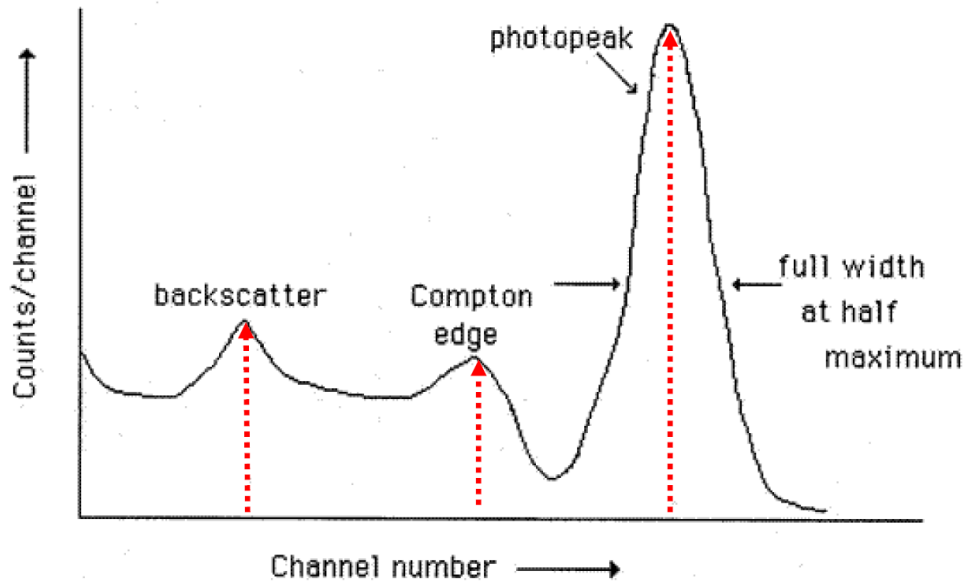


Figure 2.8. Photomultiplier spectrum that shows some processes of a gamma ray interacting with matter [28].

the incident photon. When an electron from an inner K or L shell is ejected, electrons from outer shells fall from their higher energy states to fill the vacancy [8]. The photoelectric effect is a predominant mode of interaction for gamma ray of low energies, the process is also enhanced for absorber materials of higher atomic number (Z). The approximation of the probability of the photoelectric absorption per atom is given by:

$$\tau \cong \frac{Z^n}{E_\gamma^{3.5}} \quad (2.28)$$

where exponent n varies between 4 and 5 over the gamma ray energy region of interest [9].

2.2.1.2 Compton Scattering

Compton scattering is a process in which a photon collides with a bound electron and the photon energy is considerably greater than the electron binding energy. After the interaction, the photon continues in a new direction with reduced energy and the electron attains enough energy to leave the atom. The Compton process is the most important absorption process for photons with energies of about 100 keV to approximately 20 MeV [25]. The Compton scattering results in a peak called the Compton Edge in the photomultiplier spectrum shown in Figure 2.8.

In this process, as shown in Figure 2.9, the incident gamma ray is deflected through an angle θ with respect to its original direction. A photon transfers some of its energy to the electron which is called a recoil electron, because all scattering angles are possible. The energy transferred to the electron vary from zero to a large fraction of gamma ray energy. The expression that relates the energy of the scattered photon and the scattering angle (θ) for any given interaction is given by Equation (2.29).

$$h\nu' = \frac{h\nu}{1 + \frac{h\nu}{m_0c^2}(1 - \cos(\theta))} \quad (2.29)$$

where m_0c^2 is the energy of an electron (0.511 MeV) and $h\nu$ is the energy transferred. For a small angle very little energy of a photon is transferred to an electron. Figure 2.9 shows the Compton scattering process [9].

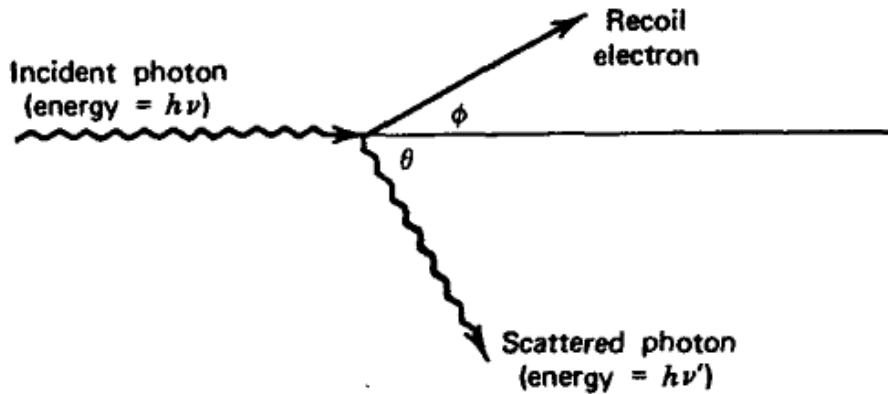


Figure 2.9. Compton Scattering [9].

2.2.1.3 Pair Production

Pair production is a process whereby an interaction of the incident γ -ray in the strong Coulomb field surrounding the nucleus results in complete transmutation of γ photon energy into an electron-positron pair. Formation of the electron-positron pair requires an energy twice the rest mass of the electron m_0c^2 , hence the pair production interaction becomes significant when the incident γ -ray energies exceed 1022 keV. The excess energy given by the photon energy minus 1022 keV (2×511 keV), is then shared between electron

and positron as kinetic energy. These particles are very short lived and they lose their kinetic energy very quickly by further collision with the electrons of the detector, followed by the spontaneous annihilation of a positron and an electron to produce two 511 keV γ -rays. For momentum to be conserved, the two photons are emitted at 180° to one another. If the detector absorbs both annihilation γ -rays, their interaction contributes to the full-energy peak in the gamma ray spectrum measured. However, if one gamma ray of the annihilation leaves the detector, the interaction contributes to the single-escape peak at 511 keV. Moreover, if both gamma rays escape, the interaction contributes to the double-escape peak which is at 1022 keV [29, 30]. Figure 2.10 shows the production of positron and electron pair.

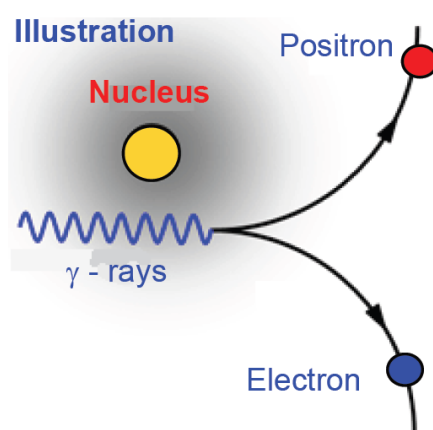


Figure 2.10. Pair production process [25].

2.3 Gamma-ray Detection

The detector is the center piece of the gamma spectroscopy system. Gamma rays interact with the detection material and transfer their energies to electrons or to positrons in the case of annihilation. Annihilation occurs when an electron (negatively charged) collides with a positron (positively charged and the electrons anti-particle) and the usual result is the emission of two gamma rays each of 511 keV, energy travelling opposite to each other.

These produced particles (positron and electron) lose their energy within the detector and create ionized atoms and ion pairs. These secondary entities form the basis of the detector signal. High purity Germanium (HPGe) is the mostly used material for gamma ray spectrometry systems [31]. More details about the available HPGe detector are discussed in Chapter 3.

In order to detect the gamma ray, the gamma ray must have an interaction with matter and that interaction must be recorded. The nature of the electromagnetic gamma ray photons allows them to have a strong interaction with electrons in the atoms of matter. The process of detecting the gamma ray is known as ionization (process by which an atom or a molecule acquires a negative or positive charge by gaining or losing electrons to form ions), where the gamma ray loses some of its energy to an electron. The electrons that are ionized, they then collide with other atoms and give out more electrons.

The released charged electron is collected either directly, which is with gas-filled detector or indirectly as with a scintillation detector. To record the present gamma ray and to measure its energy. The electrical pulse is the final result with voltage proportional to the energy transferred to the detector [32].

Three types of gamma ray detectors (Gas-filled Detectors, Scintillation Detectors and Semiconductor Detectors) are discussed on the next subsections.

2.3.1 Gas-Filled Detectors

A gas-filled detector is a metal chamber that consists of a positively biased anode wire and filled with gas. A photon travelling through the gas gives out free electrons and positive ions. The electrons are then attracted to the anode and the electric pulse is produced by the electrons. Gas counters have sensitive volume of gas between two electrodes, see Figure 2.11.

An ionization chamber is a gas-filled counter with low enough voltage between the two electrodes, that only the primary ionization charge is collected. The electrical output signal is proportional to the energy transferred to the gas volume. For the increased voltage between the electrodes, the electrons that are ionized get the kinetic energy enough to cause further ionizations. The low signal output for the ionization chamber makes this type of

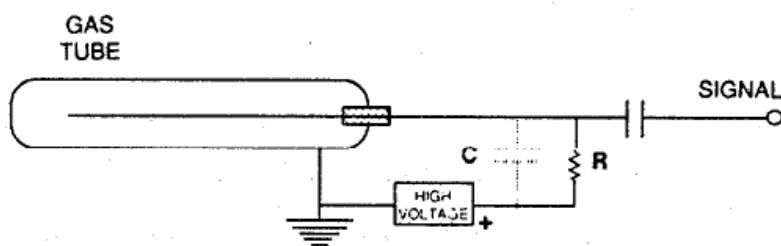


Figure 2.11. The equivalent circuit of a gas-filled detector [32].

detector very difficult to use in detecting individual gamma rays.

A proportional counter is a gas-filled detector where at high voltages the electrons are accelerated toward the anode at energies high enough to ionize other atoms, and creating a large number of electrons.

A Geiger-Mueller counter is a detector where at high voltages the multiplication of electrons is much greater and the number of electrons collected is not dependent on the initial ionization, For this detector the large output pulse is the same for all photons [33].

The different voltage regions are indicated schematically in Figure 2.12.

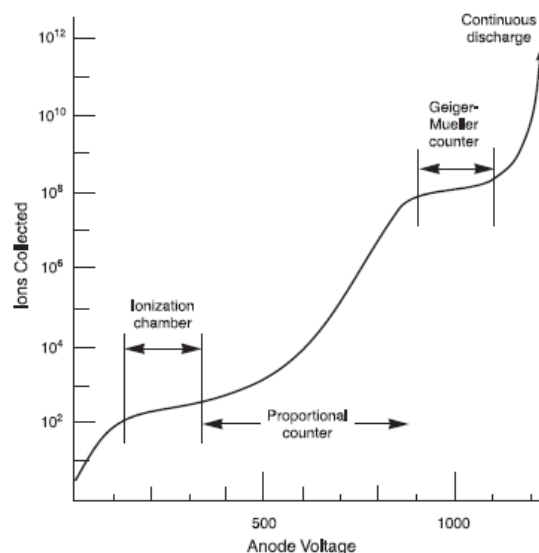


Figure 2.12. Gas Detector Output versus Anode Voltage [33].

2.3.2 Scintillation Detectors

The interaction between a gamma ray and a scintillator produces a pulse of light, which is then transformed to an electric pulse by means of a photomultiplier tube. As shown in Figure 2.13, the photomultiplier consists of a focusing electrode, a photocathode and more than 10 dynodes that multiply the number of electrons hitting them each more frequently. The dynodes and anode are biased by resistors located in a plug-on tube base assembly [33]. The common scintillator detectors are (NaI(Tl), BSO, CsI(Tl) and ZnS(Ag)). The

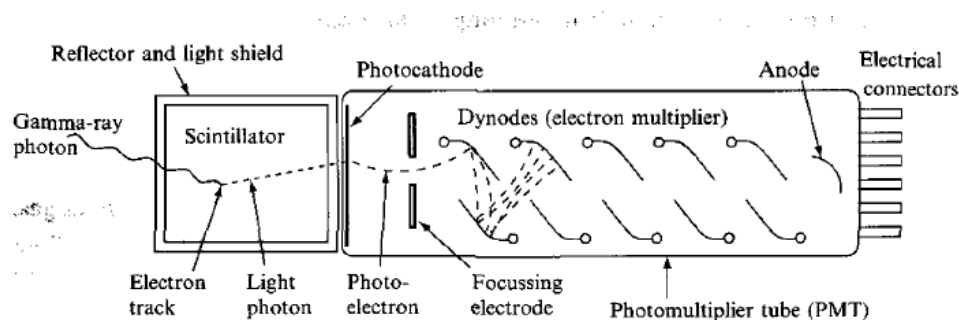


Figure 2.13. Schematic diagram of a scintillation detector [26].

important properties of the scintillator materials are light output, efficiency for stopping γ rays and the time constant (which is a measure of how quickly fluorescent light is emitted after the scintillator has been excited). Organic scintillators are effective for electrons and fast neutrons but have low γ ray detection efficiency because they have low atomic number (Z) elements [26].

2.3.3 Semiconductor Detectors

A semiconductor is a material that can act as an insulator or as a conductor [33]. A semiconductor detector consists of a crystal of a semiconductor usually silicon or germanium across which the voltage is applied. This detector appears like a solid ionization chamber where the transfer of the radiation energy to the crystal creates the electron-hole (e-h) pairs, as an inorganic scintillator. The electrons in the conduction bands (band of orbitals that are high in energy and are generally empty, in reference to conductivity in semiconductors, it is the band that accepts the electrons from the valence band) are mobile and

under the influence of applied electric field may move through crystal at a speed determined by their mobility. In a valence band, holes also move but in the opposite direction [26]. The movement of electrons and holes in a semiconductor forms a current, and if they get to their respective electrodes without recombining or becoming trapped at impurity in the crystal lattice they result in pulse of current proportion to the energy deposited in the crystal [26].

In this study a High Purity Germanium (HPGe) detector was used to detect the gamma rays from the activated bismuth discs which were irradiated. HPGe is a semiconductor detector with high energy resolution. Characteristics of the HPGe detector are high atomic number, low impurity concentration, low ionizing energy required to produce an electron-hole pair, high conductivity and first time response. Energy resolution varies with gamma-ray energies and also the size of the detector, where the energy resolution decreases with increasing gamma-ray energy and size of the Ge crystal [34].

Chapter 3

Experimental Procedures and Equipment

Measurements of cross sections for the (n,xn) reactions for the Co, Au, Bi and Tm targets using quasi mono-energetic neutron beams of 90 and 140 MeV were conducted at iThemba LABS. Subsequently, the irradiated targets were counted and analyzed using gamma-ray spectroscopy method. This chapter discusses in detail the experiments (from irradiation of the sample to counting of the radioactive sample using gamma-ray detector). Also explains the type of detector (HPGe detector) and electronic setup used to measure gamma rays in order to determine the radionuclides produced, then calculate their production cross sections.

3.1 Neutron Activation of Samples (Bi)

Neutron Activation Analysis (NAA), which was discovered in 1936, is a technique for quantitative multi-element analysis of major, minor, trace and rare elements. The first step in neutron activation analysis is irradiating a sample with neutrons in a nuclear reactor or any other type of available neutron source. The stable nucleus absorbs one neutron and becomes a radioactive nucleus. The concentration of the stable element of interest in the sample can be measured by detecting the decay of these nuclei [35]. The radioactive nuclei produced emit gamma rays, and the energies of those gamma rays are used to identify the produced nuclei. During the gamma ray measurement or spectra counting, the count

of gamma rays of a specific energy indirectly indicates the amount of an element in the sample [36].

Equation 3.1 was used in this study for the determination of a neutron cross section, which is the probability of the neutron to interact with ^{209}Bi sample and produce radioactive nuclei.

$$\sigma = \frac{A(t)}{N_0\phi(1 - e^{-\lambda t_{irr}})e^{-\lambda t_d}(1 - e^{-\lambda t_c})} \quad (3.1)$$

$A(t)$ = is the activity of a radioactive nucleus during the gamma ray measurement in Bq, N_0 = is the number of target nuclei, σ = is the cross section in cm^2 , ϕ = is the neutron flux in $\text{cm}^{-2}.\text{s}^{-1}$, λ = is the decay constant in s^{-1} , t_{irr} = is irradiation time, t_d = is delayed time and t_c = is counting time. More detailed explanation of NAA and the derivation of the above equation is discussed in Chapter 2. The details of the experiment are discussed below.

The irradiation experiments were performed at iThemba LABS using quasi-monoenergetic neutron beams via the $^7\text{Li}(p,n)^7\text{Be}$ reaction with proton beams of 92 and 142 MeV. Proton beams used in the experiment were accelerated by Separated-Sector Cyclotron (SSC) facility of iThemba LABS. Figure 3.1 shows the SSC facility which accelerates protons to energies of up to 200 MeV and heavier particles up to much higher energies. The red circled region on Figure 3.1 shows where the neutron beam facility used in this experiment is located. Figure 3.2 shows schematic view of the neutron facility.

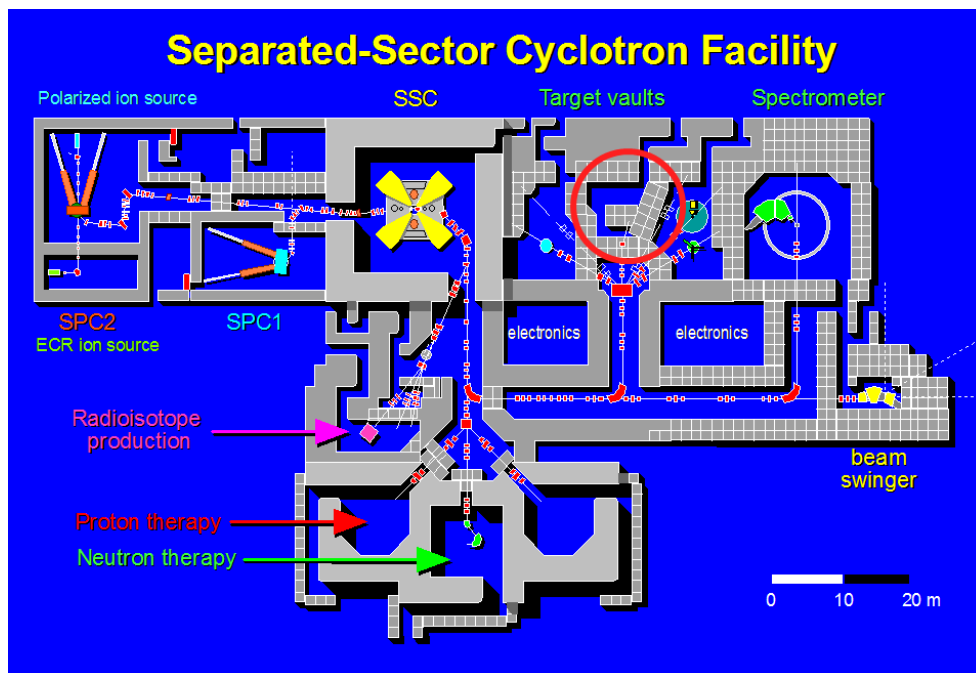


Figure 3.1. Separated-Sector Cyclotron Facility.

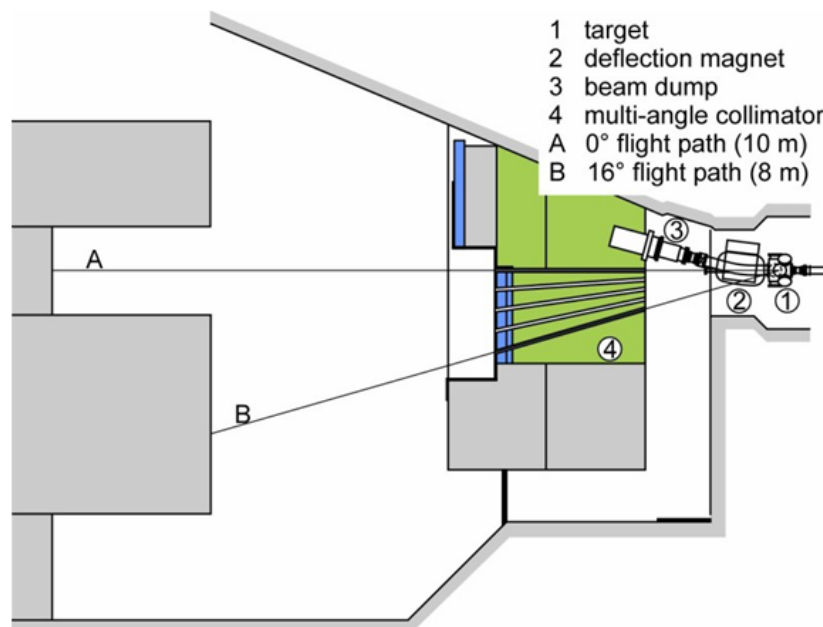


Figure 3.2. Schematic diagram of Neutron beam Facility.

The neutron production area (Li-target) is separated from the target irradiation area (Bi-target) by an iron shielding wall with collimator holes. The collimator channels have rectangular cross sections of about (48 x 48) mm² in size. At a neutron emission angle of 0° the maximum distance from the target (neutron production) is about 10 m, the beam size at this position is about (130 x 130) mm². At 16° emission angle the maximum distance is only about 8 m with a correspondingly smaller beam size. The availability of collimator at a neutron emission angle of 16° is a unique feature of this facility which allows an experimental subtraction of the detector readings effected by the neutrons from break-up continuum of the ⁷Li(p,n) reaction [37].

An example of energy spectra of the neutron beams indicated on Figure 3.3 is generated by the Li + p reaction at neutron emission angles of 0° and 16° [6]: The first component is a high energy (quasi-monoenergetic) peak, the second component is low energy continuum tail extending from the high energy peak towards lower energies. The high energy peak is dominated by the 0° spectrum but the intensity decreases as the neutron emission angle increases, the production of any radionuclide which was from (n,x) reaction produced by irradiation in the 0° beam. Therefore the 0° beam component includes reactions initiated by both the high energy peak and the continuum tail neutron beams, while the production resulting from irradiation in the 16° beam consist of the reactions initiated by the low energy continuum alone. Subtracting the yield produced in the 16° beam from that produced at 0° results in a production determined for the quasi-monoenergetic neutron energy.

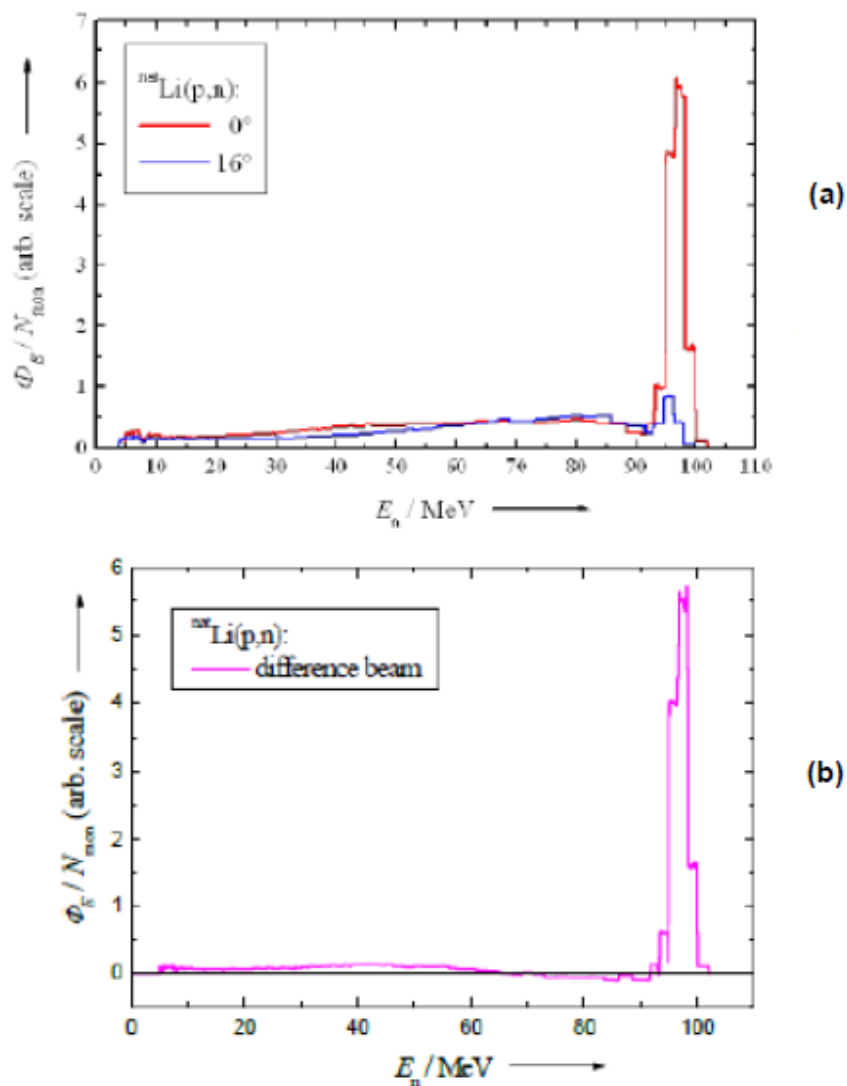


Figure 3.3. (a) Neutron time-of-flight spectra obtained after irradiating a Li-target of 5 mm thickness by proton beams of 100 MeV. The two spectra were measured at neutron emission angles of 0° and at 16° respectively and they are normalized to equalize the total number of counts in the continuum region. (b) Difference spectrum obtained by subtracting the 16° spectrum from the 0° spectrum [6]

3.1.1 Target Specifications

As was mentioned earlier on, measurements of cross sections for neutron induced reactions on Bi target were conducted using proton beams of 92 and 142 MeV, with the proton energy loss in the Li (8 mm) target of about 2 MeV depending on the thickness of Li-target, neutrons produce from (p,n) reaction are of 90 and 140 MeV. Stacked samples of ^{nat}Al , ^{nat}Cu , ^{59}Co , ^{197}Au , ^{169}Tm and ^{209}Bi were irradiated at the iThemba LABS neutron beam facility using neutron energies of about 90 MeV and 140 MeV. Two identical target stacks were irradiated simultaneously for each measurement, one in the 0° beam line and the other in the 16° beam line. Figure 3.4 shows how the targets were stacked during irradiation, where x samples refer to (Co, Au, Tm and Bi) targets. Both the Al and Cu samples were used as monitor targets. Figure 3.5 is a photograph of the experimental set up showing the stacked target at (a) 0° and (b) 16° . This work focuses on reporting about neutron cross sections for ^{209}Bi target only.

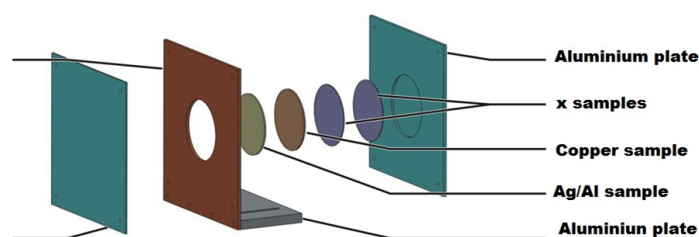


Figure 3.4. Illustration of how targets were stacked during experiment.



Figure 3.5. A photograph of the experimental setup showing the stacked target at (a) 0° and (b) 16° .

Target materials (Co, Au, Tm and Bi) were in a form of thin discs with diameter of 25 mm and about 0.5 mm thickness. As per manufacturer (GoodFellow Corp.) specifications, all target materials supplied were 99.9% pure. Target materials were placed at 5 m away from the Li target and irradiation time of about 15-40 hrs. Laser beams were used to align the centre of the target with the neutron beam line. After the irradiation experiments, four activated discs (labelled: Bi_1, Bi_2, Bi_3 and Bi_4) were ready for counting in the HPGe system and analyzed.

Bi_1 is ^{209}Bi target that was placed at 0° neutron emission angle and was bombarded with 90 MeV neutron beam. **Bi_2** is ^{209}Bi target that was placed at 16° neutron emission angle and was bombarded with 90 MeV neutron beam. **Bi_3** is ^{209}Bi target that was placed at 0° neutron emission angle and was bombarded with 140 MeV neutron beam. And **Bi_4** is ^{209}Bi target that was placed at 16° neutron emission angle and was bombarded with 140 MeV neutron beam. The energy, target and the angle at which the target was bombarded are summarized in Table 3.1

Table 3.1. Table that shows the activated discs (labelled: Bi_1, Bi_2, Bi_3 and Bi_4) after the irradiation experiment.

Energy (MeV)	Target	Angle
90	Bi_1	0°
	Bi_2	16°
140	Bi_3	0°
	Bi_4	16°

3.2 Gamma-ray Spectroscopy

In this section the gamma ray energy measurement is discussed in detail as well as the electronics which were used in the detection of gamma rays using HPGe detector.

3.2.1 Energy Measurements

Figure 3.6 shows the schematic diagram of electronic equipment that was used to measure the energy of nuclear radiations emitted by a source. The electronic signal from the detector

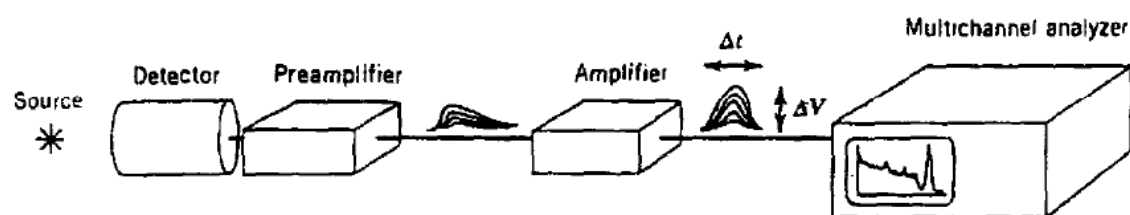


Figure 3.6. Schematic diagram of electronic equipment that is used in a measurement of the energies of radiations emitted by a source [7].

went directly to preamplifier which transformed the charge pulse from the detector to a voltage pulse (i.e by charging the capacitor) and then the pulse was taken to the next element in the circuit. The amplifier was there to provide the voltage gain to bring the millivolt preamp pulse to the range of few volts where it could be processed. The amplifier might be linear so that the proportionality of radiation energy and pulse height could be preserved. The many pulse heights that might be produced by a decay process were then displayed on MultiChannel Analyzer (MCA) in histogram style, that was with pulse height on the horizontal scale and number of pulses on the vertical scale. The input pulses were then digitized and the digital pulse height was stored in a memory location referred to as a channel, then the horizontal axis was labeled as channel number. The resulting pulse-height spectrum could then be used to determine the energies of the radiations emitted by the source (from the locations on the horizontal scale) and their relative intensities (from the area of the different peaks in the spectrum) [7]. This was the process used when analysing or determining the gamma ray energy from the spectrum.

3.2.2 ERL High Purity Germanium (HPGe) Detector

The activated samples were measured by means of gamma-ray spectroscopy using a High Purity Germanium (HPGe) detector system. The specifications of the Environmental Radioactivity Laboratory (ERL) of iThemba LABS HPGe detector used for gamma-ray measurements were as follow (see also Figure 3.7), a Canberra p-type detector with 45% relative efficiency, 2.2 keV resolution at 1332 keV and placed in a low-background setup, see Figure 3.7 and 3.8.

The detector was covered in a 10 cm thick lead castle fitted with a 2.0 mm thick copper inner lining in order to reduce the background in the sample spectra. A gamma-ray was emitted from the sample and entered the detector where it undergoes number of interactions resulting in the ionisation of the germanium atoms in the detector crystal. The crystal of the detector was operating under a vacuum and therefore small amounts of moisture which might leak into the system could contaminate the crystal. Therefore, liquid nitrogen was used to minimise the thermal noise of the detector and to freeze any kind of moisture in the system in order to maintain the vacuum. It was therefore very important that the liquid nitrogen supply was continuously maintained to prevent the system from warming up, which could cause moisture and short-circuiting of the system and damaging the detector.

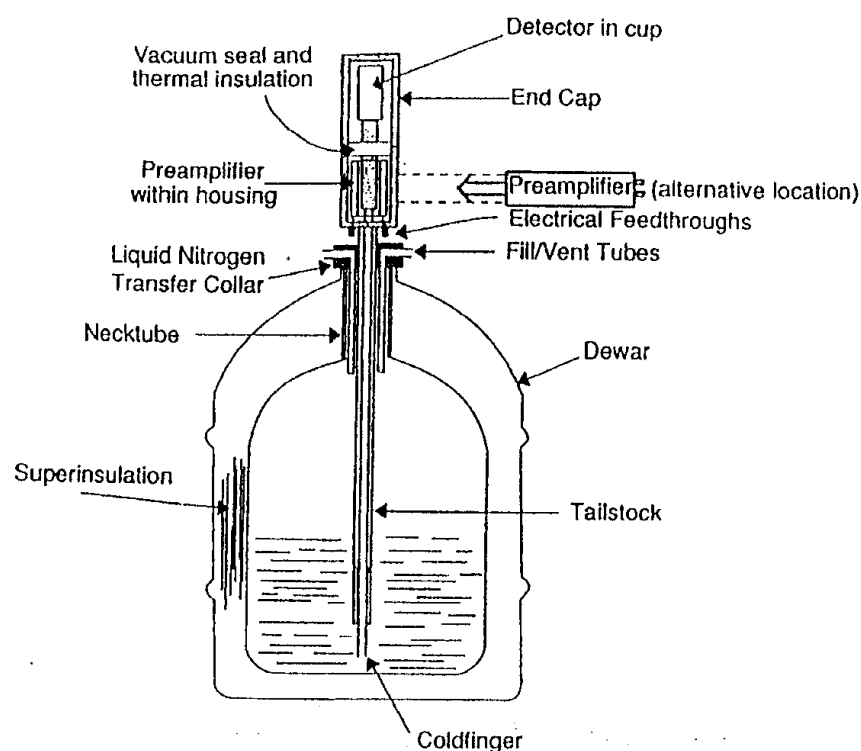


Figure 3.7. Cross-section diagram of HPGe detector with liquid nitrogen reservoir [?].



Figure 3.8. A photograph of the ERL iThemba LABS High Purity Germanium Detector.

The detector system and electronic setup used for collecting data which was to acquire gamma ray spectra is shown in Figure 3.9. The pulses from the amplifier were collected and sorted by the ATOMKI Palmtop software Multi-Channel Analyzer (MCA). The output was in a form of a display (spectrum) of number of counts and the corresponding channel numbers displayed on the y and x axis respectively. The system was energy and efficiency calibrated regularly with a certified reference sources such that the centroid of the photo-peaks and the gamma-ray detection efficiency were continuously monitored.

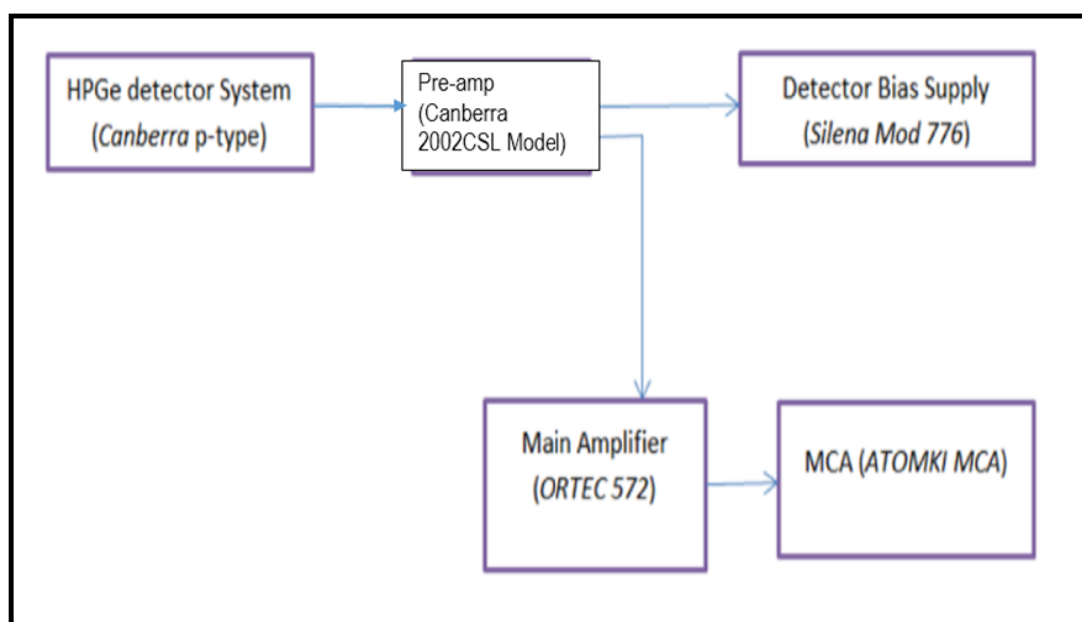


Figure 3.9. Schematic diagram of electronic setup of the ERL HPGe detector system.

For efficiency calibration of the detector, certified reference point sources (^{152}Eu -1209(62) Bq, ^{137}Cs -1322(46) Bq and ^{60}Co -1073(36) Bq) were used and all were prepared by NMISA on 01 September 2014. A power fit was then used to calculate the efficiency calibration parameters. Furthermore, efficiency calibrations were also calculated using the MCNPX simulation code and compared with experimental data for estimation of various measuring geometries where standard radiation sources were not available. Energy and efficiency calibration are discussed in subsections 3.2.3 and 3.2.4 respectively.

3.2.3 Energy Calibration

The ERL HPGe system was calibrated weekly with an IAEA reference sources (Thorium-Th and Potassium chloride-KCl). The photo peak energy (E) in Equation (3.2) represents a linear function of channel number (x), where A and B are energy calibration parameters.

$$E = A + B * x \quad (3.2)$$

The regions of interest (ROI) are manually set on the spectrum. The parameters B and A are determined by using least-squares fit to the calibration points and corresponding to the gradient and intercept of the calibration line. In the MCA system, one is able to specify the energy associated with each relevant centroid channel corresponding to a particular region of interest. The plot of energy calibration is shown in Figure 3.10, where A and B parameters are found to be -1.2404 and 0.522 respectively.

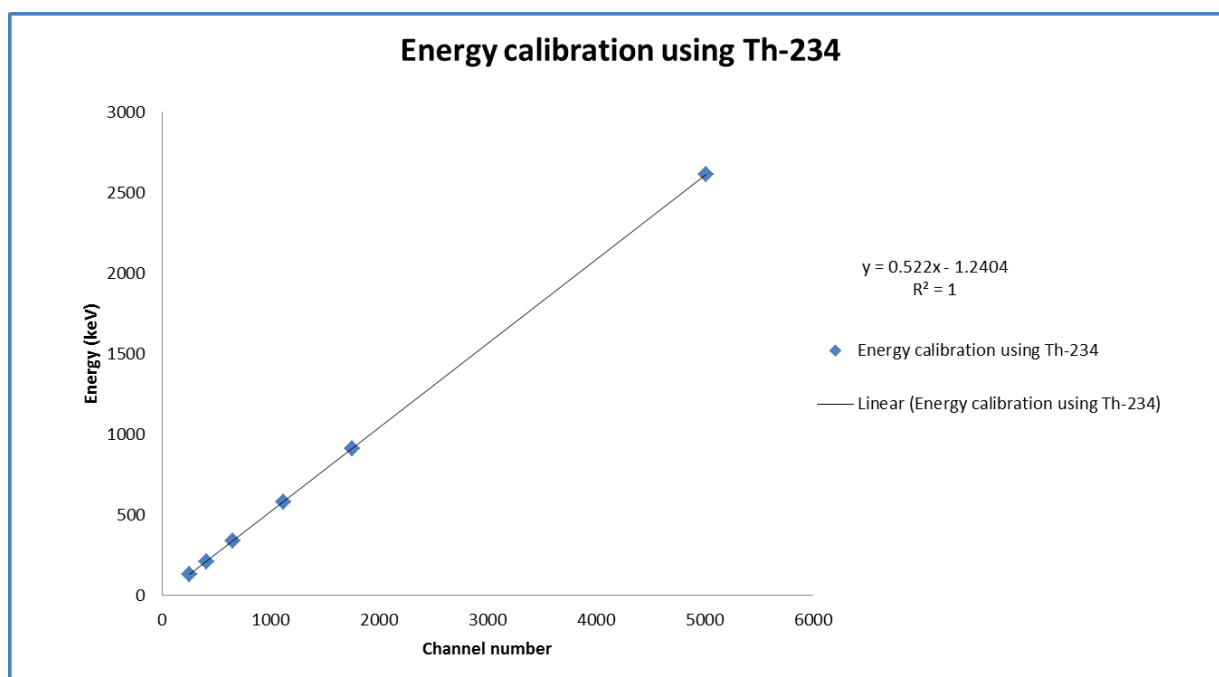


Figure 3.10. Energy Calibration plot obtained using Th-234 source.

3.2.4 Efficiency Calibration

For gamma spectrometric analysis, efficiency calibration of a gamma ray detector was carried out using a set of certified reference point sources. Gamma rays emitted by point sources (^{152}Eu , ^{60}Co and ^{137}Cs) were measured using HPGe detector. Examples of the acquired gamma ray spectra are shown Figures 3.11, 3.12 and 3.13.

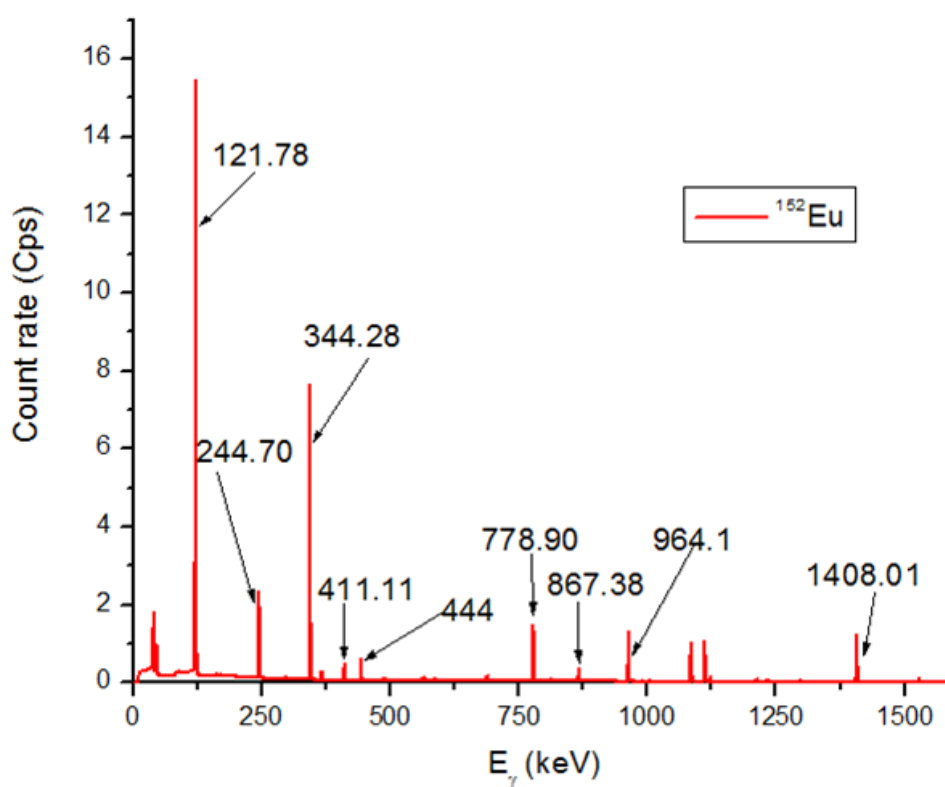


Figure 3.11. Gamma ray spectrum of ^{152}Eu point source.

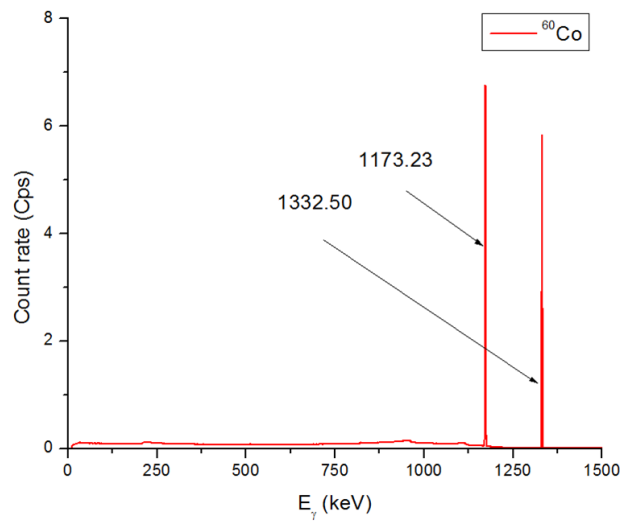


Figure 3.12. Gamma ray spectrum of ^{60}Co point source.

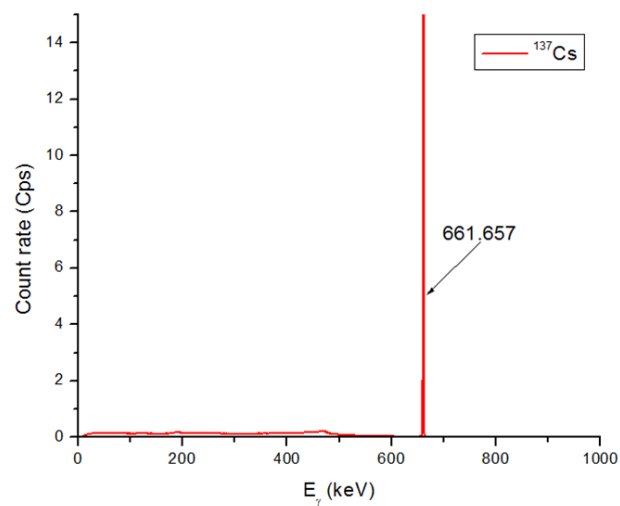


Figure 3.13. Gamma ray spectrum of ^{137}Cs point source.

The spectra for known sources were then used in determining the efficiency and parameters of the detector.

3.2.5 Determination of Efficiency of the Detector.

After gamma energies were identified from the spectra of the known sources, the efficiency value was calculated taking into account the probability of disintegration (branching ratio) for each energy. Equation (3.3) was used to calculate the efficiency of the detector, the calculated efficiency is shown in a form of a graph in Figure 3.14.

$$\varepsilon(E) = \frac{\text{counts}}{A * Br * t} \quad (3.3)$$

where $\varepsilon(E)$ is the detector efficiency at given energy (E).

counts is number of counts at given energy and background corrected.

A is the activity of the known source (Bq).

t is counting time.

Br is branching ratio.

The initial activities (A_o) that was used to calculate the present activities (A) for each point source were given i.e ($^{152}\text{Eu} = 1209(62)$ Bq, $^{60}\text{Co} = 1073(36)$ Bq and $^{137}\text{Cs} = 1322(46)$ Bq). The present activity is given by Equation (3.4).

$$A = A_o e^{-\lambda t} \quad (3.4)$$

where λ is decay constant, which is calculated using Equation (3.5).

t is $t_{\text{present}} - t_{\text{initial}}$.

$$\lambda = \frac{\ln(2)}{t_{\frac{1}{2}}} \quad (3.5)$$

where $t_{\frac{1}{2}}$ is half life of the known source. After calculating the present activity (A) for each point source, the efficiency of the detector for each gamma ray energy using Equation (3.3) was calculated. Table 3.2 show the results of the calculated efficiency of detector as a fuction of energy. The efficiency results are shown in a form of a graph in Figure 3.14, the fit was in the form of $\varepsilon(E) = cE^{-d}$, where $\varepsilon(E)$ was the efficiency as the function of energy and (c and d) were parameters which were found to be 4.544 and 0.73 respectively. The

parameters (c and d) were then used to calculate the efficiency as a function of energy for any point source (irradiated discs included) counted using the ERL HPGe detector system.

Table 3.2. Determination of the detector efficiency using (^{152}Eu , ^{60}Co and ^{137}Cs) certified reference point sources.

Radionuclides	Energy (KeV)	Braching ratio	Activity (Bq)	Efficiency	Uncertainty
^{152}Eu	121.78	0.2837	1141.55	0.1282	0.0066
	244.69	0.0753	1141.55	0.0776	0.0039
	344.27	0.2657	1141.55	0.0728	0.0037
	778.90	0.1297	1141.55	0.0344	0.0018
	867.37	0.0421	1141.55	0.0248	0.0013
	964.10	0.1463	1141.55	0.0289	0.0015
	1085.84	0.1013	1141.55	0.0304	0.0016
	1112.07	0.1354	1141.55	0.0278	0.0014
	1212.95	0.0141	1141.55	0.0201	0.0010
	1299.14	0.0163	1141.55	0.0227	0.0012
1408.01	0.2085	1141.55	0.0228	0.0012	
^{137}Cs	661.48	0.8510	1287.91	0.04836	0.0017
^{60}Co	1172.92	0.9990	924.08	0.02923	0.0009
	1332.15	0.9998	924.08	0.02617	0.0009

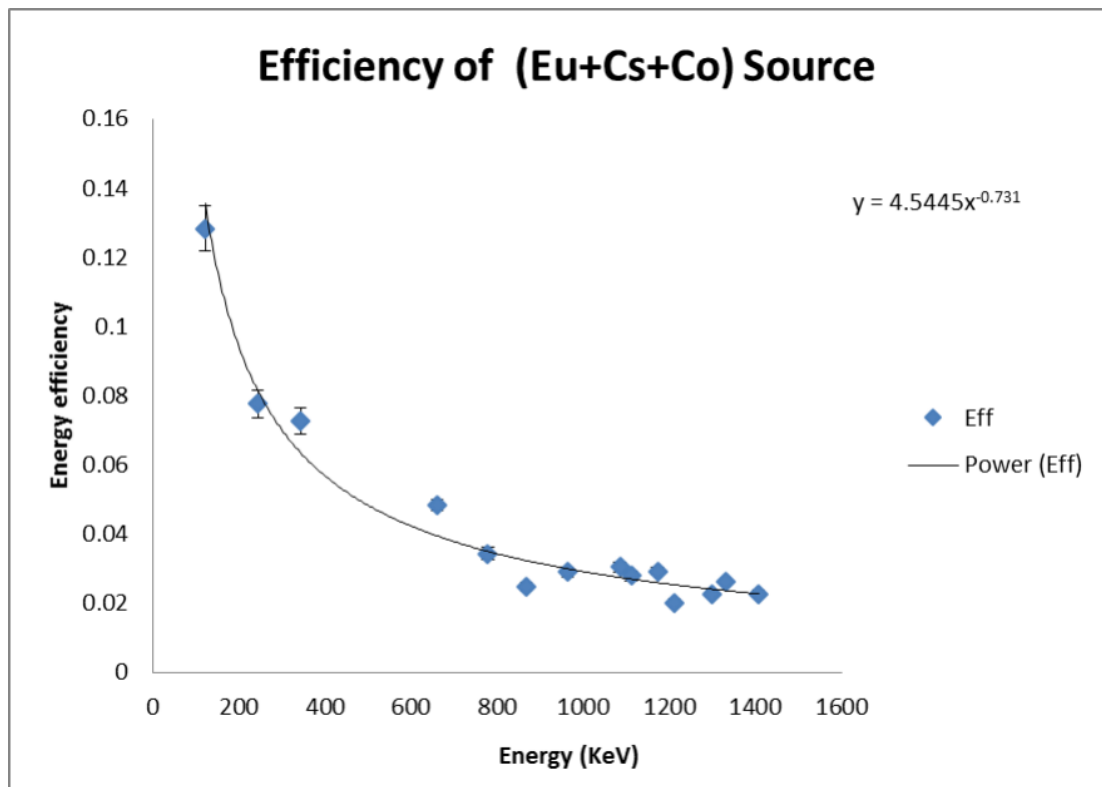


Figure 3.14. Efficiency of the detector for each gamma-ray energy of the sources (^{152}Eu , ^{60}Co and ^{137}Cs).

Chapter 4

Data Analysis, Results and Discussions

4.1 Identification of Radionuclides using Gamma-ray Spectroscopy

The aim of this work was to measure the neutron cross section of the following reactions $^{209}\text{Bi}(n,3n)^{207}\text{Bi}$, $^{209}\text{Bi}(n,4n)^{206}\text{Bi}$, $^{209}\text{Bi}(n,5n)^{205}\text{Bi}$, $^{209}\text{Bi}(n,6n)^{204}\text{Bi}$, $^{209}\text{Bi}(n,7n)^{203}\text{Bi}$ and $^{209}\text{Bi}(n,8n)^{202}\text{Bi}$. Two weekends (20 September 2014 - 22 September 2014 and 27 September 2014 - 29 September 2014) were allocated for beam time. While first weekend was for irradiation using 90 MeV neutrons, the second weekend was allocated for 140 MeV neutrons. After the experiments (irradiation of targets) were performed at iThemba LABS neutron beam facility, radioactive discs were taken to the ERL HPGe dectector for gamma ray measurements. However due to the fact that there was only one HPGe detector available at the ERL for measuring gamma rays, only one radioactive disc was counted at a time which resulted in decay of some of the short-lived radionuclides produced such as ^{202}Bi -(11.22 hrs), ^{203}Bi -(11.76 hrs) and ^{204}Bi -(1.72 hrs). Therefore, only radionuclides with relative long half lifes such as (^{207}Bi - 31.55 yrs, ^{206}Bi - 6.243 days, ^{205}Bi - 15.31 days) were identified from the gamma ray spectra.

The level schemes for the decay of radionuclides (^{205}Bi , ^{206}Bi and ^{207}Bi) were used to study the decay of each radionuclide and record the energy of the emitted gamma rays and their branching ratios. Figure 4.1 shows an example of the decay of ^{207}Bi level scheme [38].

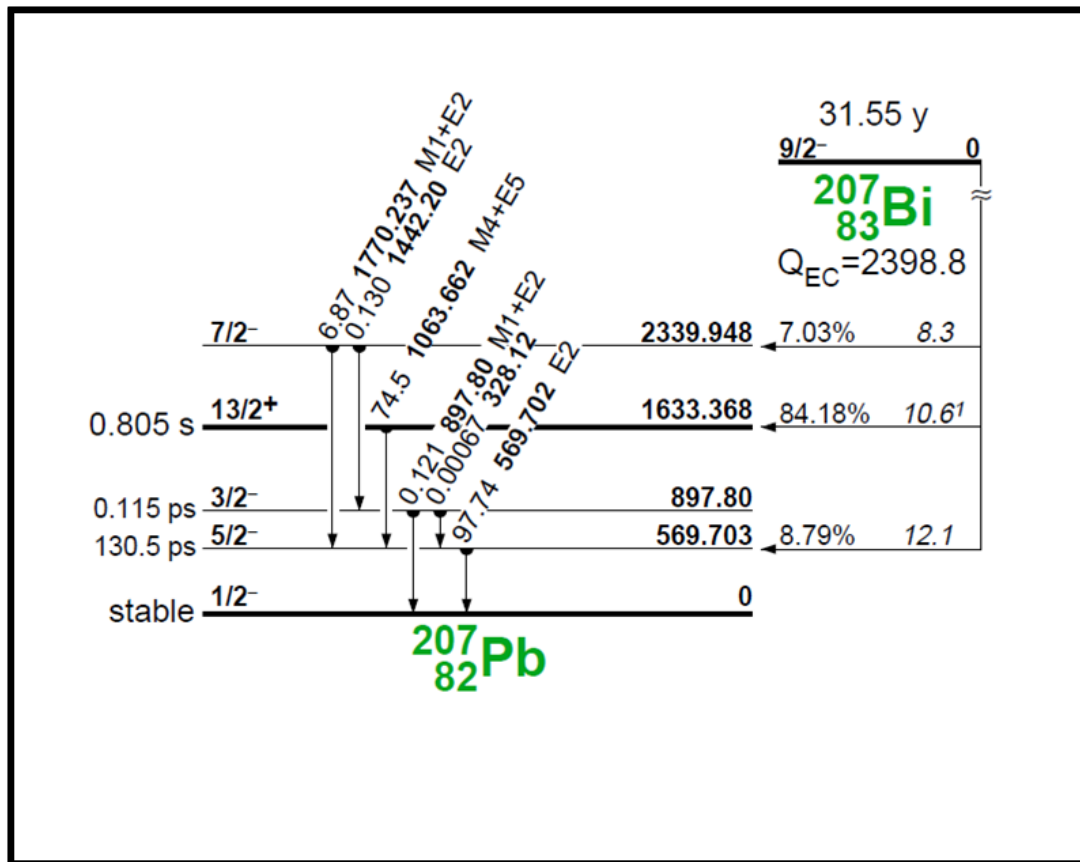


Figure 4.1. Level scheme of the decay of ^{207}Bi [38].

Figure 4.2 shows the full spectra acquired from two activated Bi discs (one was placed at 0° and the other was placed at 16°). The spectra in Figure 4.2 refers to discs irradiated in the first weekend ($E_n \approx 90$ MeV), and are superimposed on the measured background of the ERL system.

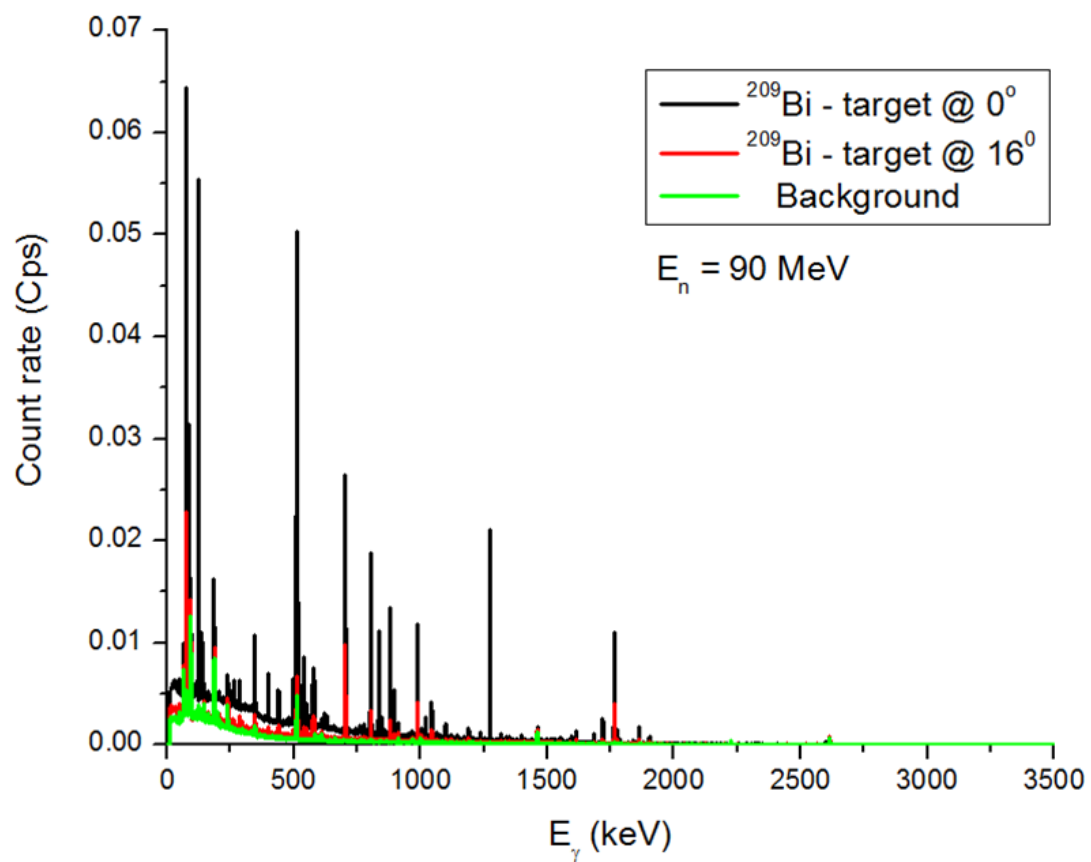


Figure 4.2. Full gamma ray spectrum of $^{209}\text{Bi}(n, xn)$ reaction where neutron beam of 90 MeV energy was used.

The spectra in Figure 4.3, 4.4 and 4.5 show various regions of interests and indicate the identified radionuclides.

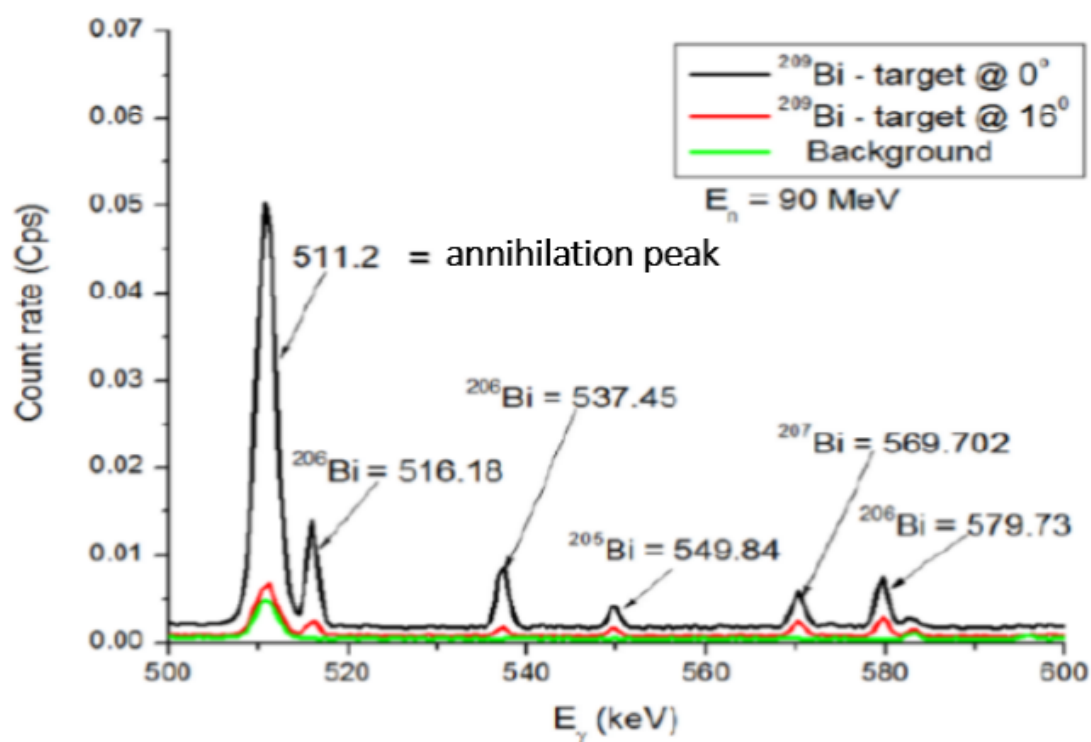


Figure 4.3. Selected region (500 - 600 keV) for $^{209}\text{Bi}(n,xn)$ reaction spectrum showing the identified 511 keV annihilation peak and the identified ^{205}Bi , ^{206}Bi and ^{207}Bi radionuclides.

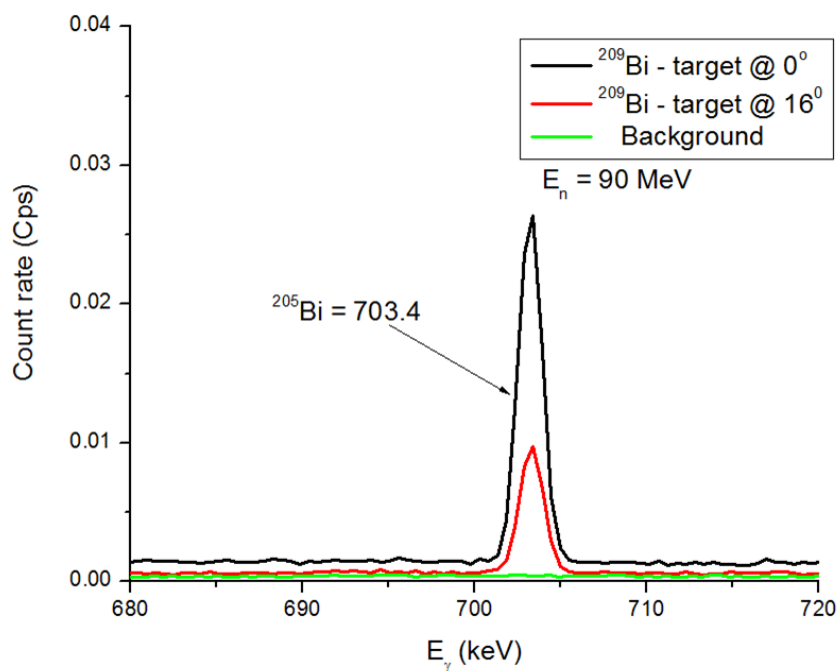


Figure 4.4. Selected region (680 - 720 keV) showing $^{209}\text{Bi}(n,5n)^{205}\text{Bi}$ reaction 703.5 keV photopeak.

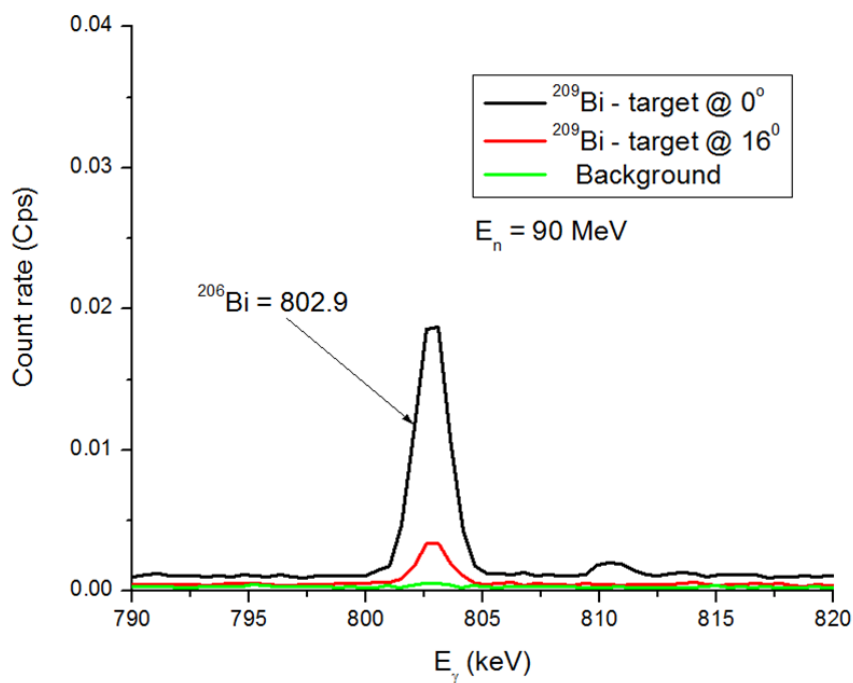


Figure 4.5. Selected region (790 - 820 keV) showing $^{209}\text{Bi}(n,4n)^{206}\text{Bi}$ 802.9 keV reaction photopeak.

Figure 4.6 shows the full spectra acquired from activated Bi discs (one was placed at 0° and the other was placed at 16° neutron emission angle), and discs were irradiated using neutrons of 140 MeV energy.

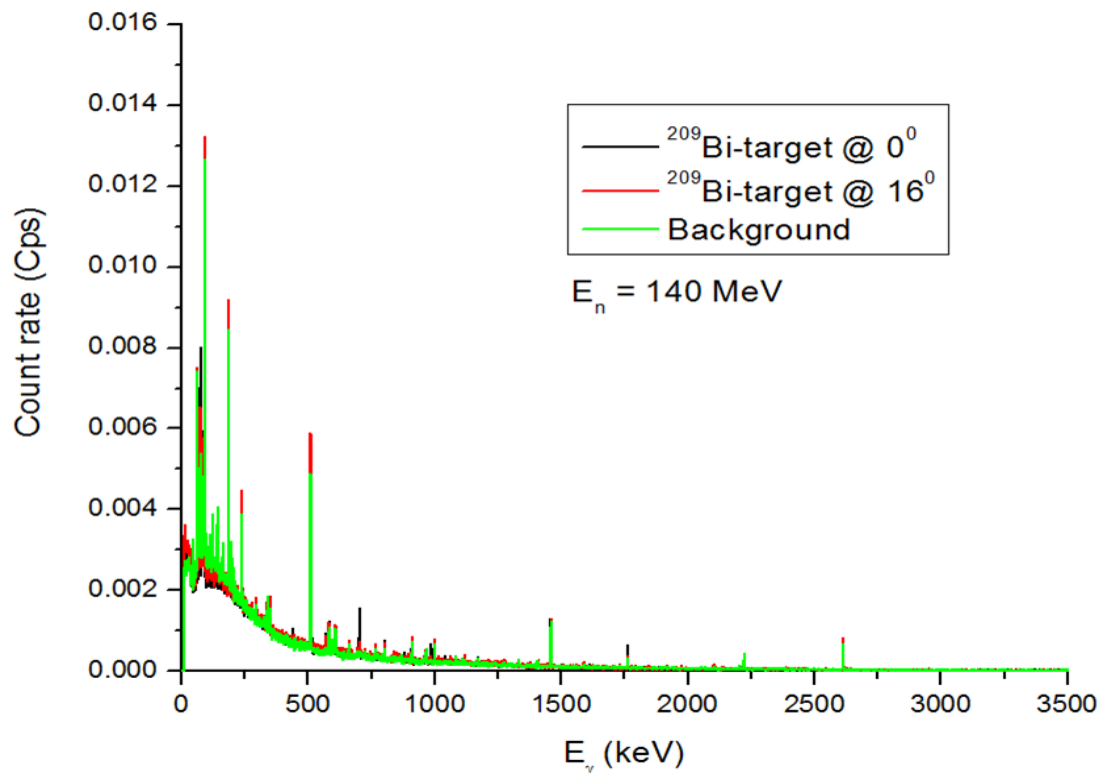


Figure 4.6. Full gamma ray spectrum of $^{209}\text{Bi}(n,xn)$ reaction where neutron beam of 140 MeV energy was used.

The spectra in Figure 4.7, 4.8 and 4.9 show various regions of interests and indicate the identified ^{205}Bi , ^{206}Bi and ^{207}Bi radionuclides.

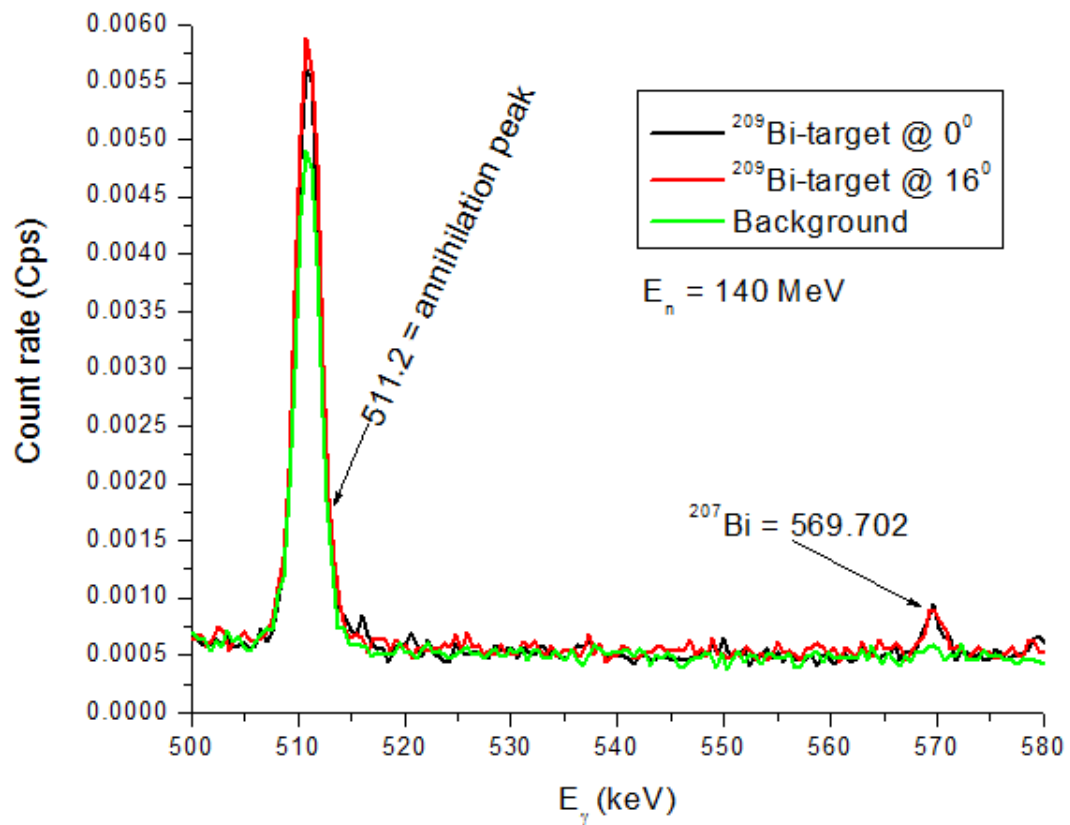


Figure 4.7. Selected region (500 - 580 keV) showing $^{209}\text{Bi}(n,3n)^{207}\text{Bi}$ reaction photopeak and 511 keV annihilation peak.

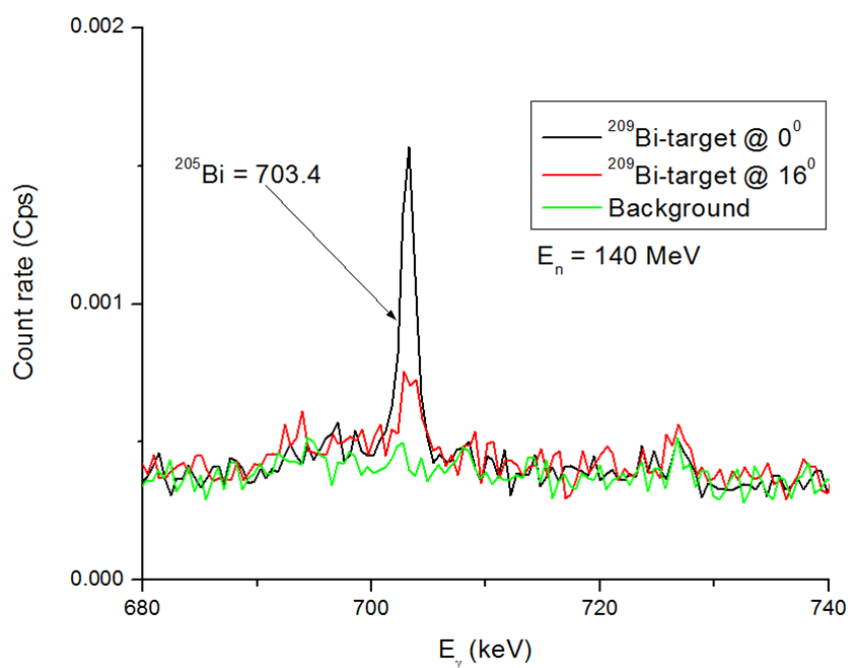


Figure 4.8. Selected region (680 - 740 keV) showing $^{209}\text{Bi}(n,5n)^{205}\text{Bi}$ reaction 703.4 keV photopeak.

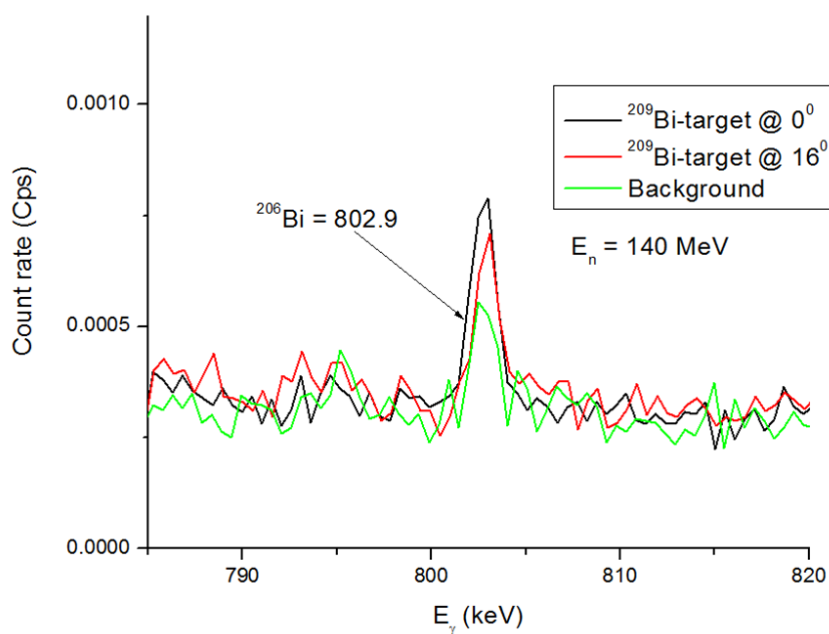


Figure 4.9. Selected region (760 - 820 keV) showing $^{209}\text{Bi}(n,4n)^{206}\text{Bi}$ reaction 802.9 keV photopeak.

During the study of the gamma ray spectra, it was observed that the peaks of spectrum acquired from 0° are more enhanced compared to the peaks from 16° , that is because the neutron beams that were collimated from 16° during the irradiation were dominated by the low energy neutron beams. While at 0° only high energy neutron beams were collimated. Therefore reactions that were initiated by neutron beams from 16° produced peaks with background contamination, while the reactions that were initiated by neutron beams from 0° produce only the peaks of interest.

After the identification of radionuclides (^{205}Bi , ^{206}Bi and ^{207}Bi), the next step was to determine the cross section which was the probability of producing these nuclides.

4.2 Determination of the Activity of radionuclides

Activity of a radionuclide measures the number of radioactive disintegrations or transformations an amount of material undergoes in a given period of time and it changes in time [39].

The efficiency calculated in subsection 3.2.4 was used to determine the activity of a radionuclide present. Equation (4.1) was used to calculate activity of radionuclide and Equation (4.2) was used to estimate the uncertainty of the activity, where eff_{error} is the error of the efficiency and $Counts_{error}$ is the error of the counts rate.

$$A = \frac{Counts}{\varepsilon * Br * t} \quad (4.1)$$

$$A_{error} = A * \sqrt{\left(\frac{eff_{error}}{eff}\right)^2 + \left(\frac{Counts_{error}}{Counts}\right)^2} \quad (4.2)$$

After calculating the activity, the average activity of each radionuclide was then calculated.

Table 4.1. Activity and weighted average activity of radionuclides produced from ^{209}Bi that was irradiated with 90 MeV neutron beam.

Radio-nuclides	Energy (keV)	Branching ratio	0		16	
			Activity (Bq)	Average Activity	Activity (Bq)	Average Activity
^{205}Bi	549.85	0.0295	6.05 ± 0.77	6.65 ± 0.74	2.57 ± 0.14	2.66 ± 0.14
	570.60	0.0434	6.84 ± 0.43		2.83 ± 0.14	
	579.73	0.0544	5.89 ± 0.37		2.36 ± 0.12	
	703.44	0.31	7.58 ± 0.38		2.80 ± 0.14	
	987.62	0.1613	8.77 ± 0.45		3.29 ± 0.16	
	1043.72	0.0751	5.76 ± 0.36		2.15 ± 0.11	
^{206}Bi	516.18	0.407	1.77 ± 0.09	1.99 ± 0.18	0.20 ± 0.01	0.31 ± 0.02
	537.35	0.305	1.59 ± 0.09		0.27 ± 0.01	
	803.10	0.99	1.95 ± 0.09		0.32 ± 0.02	
	881.01	0.662	2.10 ± 0.11		0.32 ± 0.02	
	895.12	0.1566	3.28 ± 0.19		0.51 ± 0.03	
	1718.70	0.318	1.96 ± 0.11		0.26 ± 0.02	
^{207}Bi	569.70	0.9774	0.31 ± 0.02	0.151 ± 0.04	0.14 ± 0.01	0.097 ± 0.12
	1063.66	0.745	0.04 ± 0.01		0.20 ± 0.01	
	1770.24	0.0687	0.09 ± 0.09		0.06 ± 0.34	

The calculated activity results presented in Tables 4.1 are shown schematically in plots indicated by Figures 4.10 - 4.12.

Figures 4.10 - 4.12 show the plots for activity and the weighted average activity for ($^{209}\text{Bi}(n,3-5n)$) reactions, where neutron beam of 90 MeV was used and target was placed at 0° and 16° neutron emission angles.

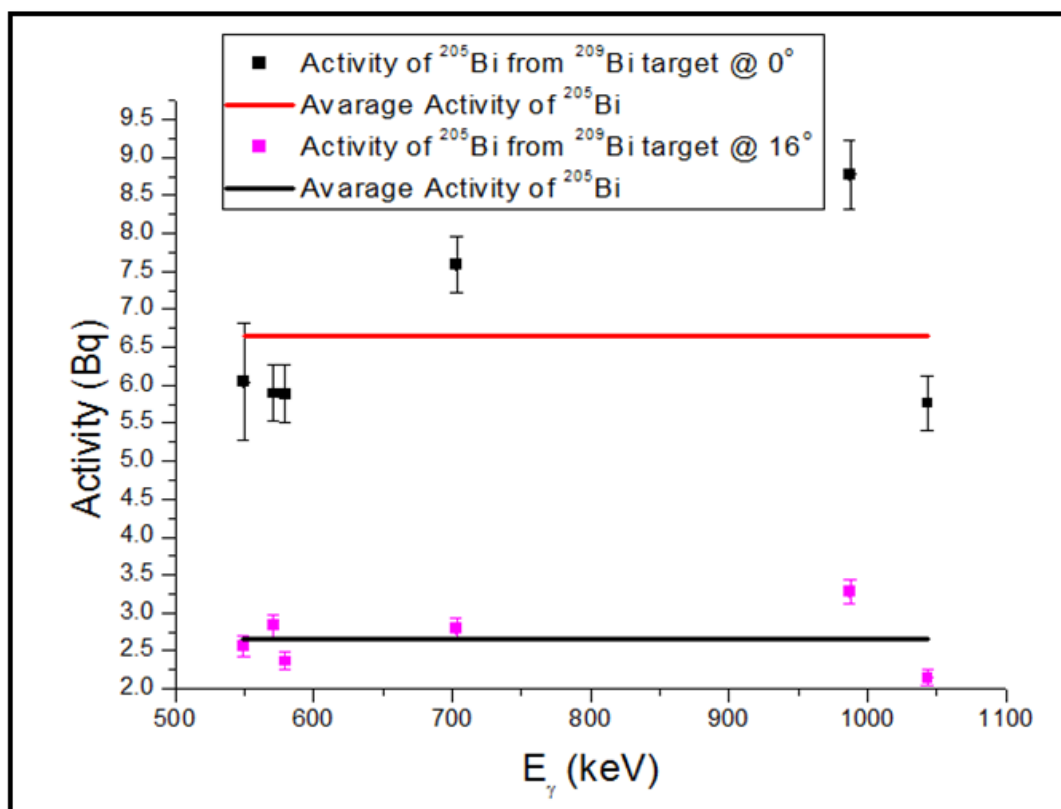


Figure 4.10. The activity (Bq) of ^{205}Bi radionuclide as a function of energy for the reaction of $^{209}\text{Bi}(n,5n)$ at neutron beam energy of 90 MeV.

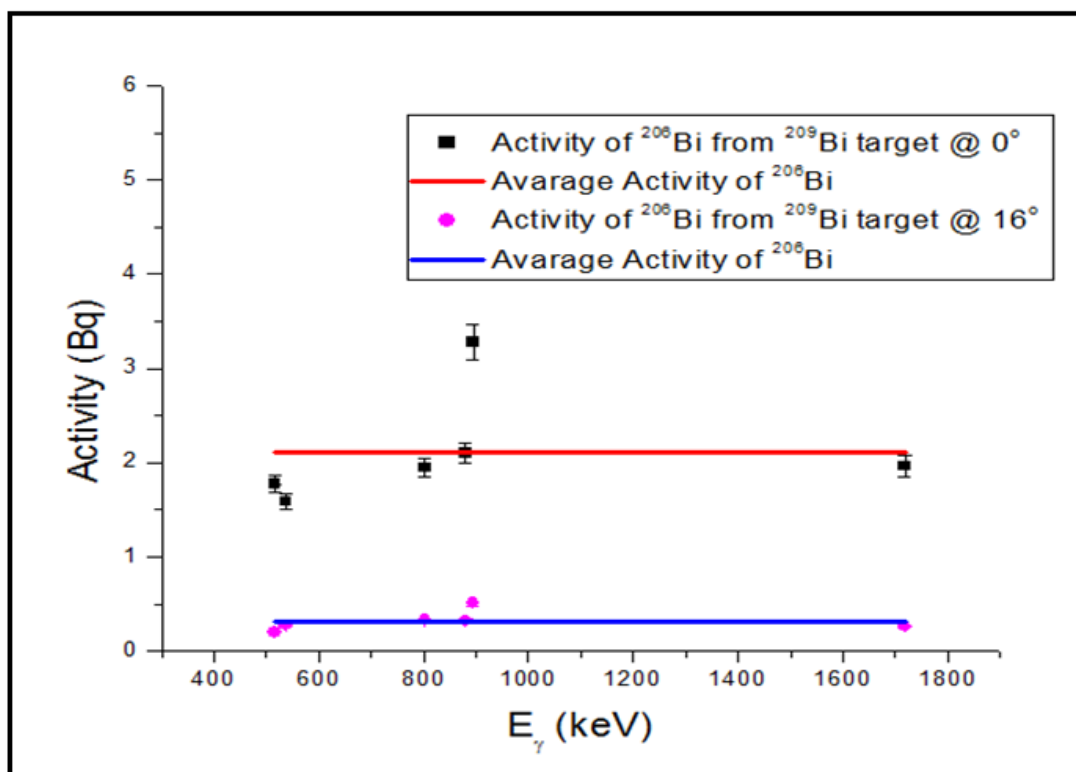


Figure 4.11. The activity (Bq) of ²⁰⁶Bi radionuclide as a function of energy for the reaction of ²⁰⁹Bi(n,4n) at neutron beam energy of 90 MeV.

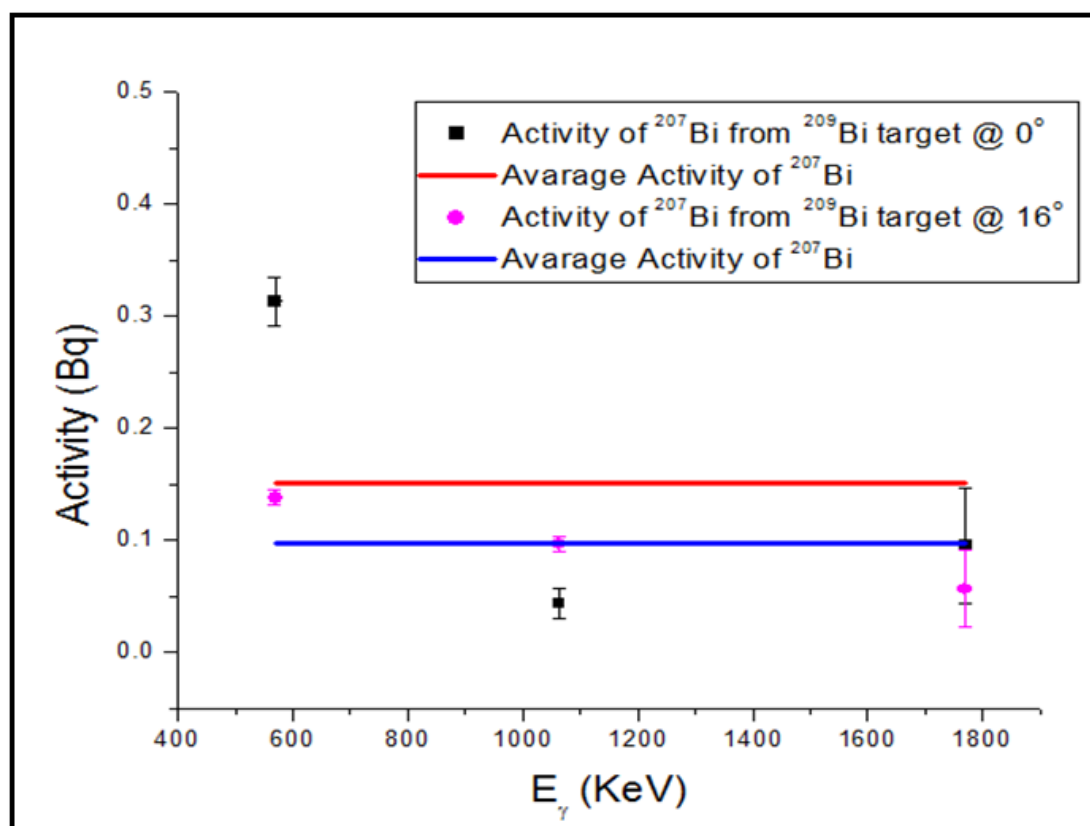


Figure 4.12. The activity (Bq) of ²⁰⁷Bi radionuclide as a function of energy for the reaction of ²⁰⁹Bi(n,3n) at neutron beam energy of 90 MeV.

After this analysis it was observed that the activity was higher for the radionuclides produced from the reactions where a target was placed at 0°, while the activity for the reactions where a target was placed at 16° is lower. This is because neutron beam that initiated the reactions where the target was placed at 0° was of the high energy only without any contaminants, whereas the neutron beam that initiated the reactions where the target was placed at 16° was of low energy.

Table 4.2. Activity and weighted average activity of radionuclides produced from ^{209}Bi that was irradiated with 140 MeV neutron beam.

Radio-nuclides	Energy (keV)	Branching ratio	90		16	
			Activity (Bq)	Average Activity	Activity (Bq)	Average Activity
^{205}Bi	549.85	0.0295	0.31 ± 0.08	0.51 ± 0.04	0.40 ± 0.21	0.49 ± 0.09
	570.60	0.0434	0.33 ± 0.05		0.46 ± 0.06	
	579.73	0.0544	0.32 ± 0.05		0.41 ± 0.05	
	703.44	0.31	0.34 ± 0.02		0.50 ± 0.03	
	987.62	0.1613	0.39 ± 0.02		0.52 ± 0.12	
	1043.72	0.0751	0.36 ± 0.05		0.46 ± 0.06	
^{206}Bi	516.18	0.407	0.02 ± 0.008	0.0358 ± 0.02	0.02 ± 0.008	0.029 ± 0.02
	537.45	0.305	0.04 ± 0.01		0.01 ± 0.03	
	803.10	0.99	0.046 ± 0.002		0.033 ± 0.004	
	881.01	0.662	0.034 ± 0.004		0.02 ± 0.01	
	895.12	0.1566	0.03 ± 0.003		0.03 ± 0.02	
	1718.70	0.318	0.04 ± 0.02		0.02 ± 0.01	
^{207}Bi	569.70	0.9774	0.040 ± 0.002	0.049 ± 0.05	0.031 ± 0.003	0.039 ± 0.08
	1063.66	0.745	0.027 ± 0.004		0.02 ± 0.01	
	1770.24	0.0687	0.08 ± 0.15		0.06 ± 0.24	

Figures 4.13 - 4.15 indicate reactions ($^{209}\text{Bi}(n,3-5n)$), where neutron beam of 140 MeV energy was used and target was placed at (0° and 16°) neutron emission angle.

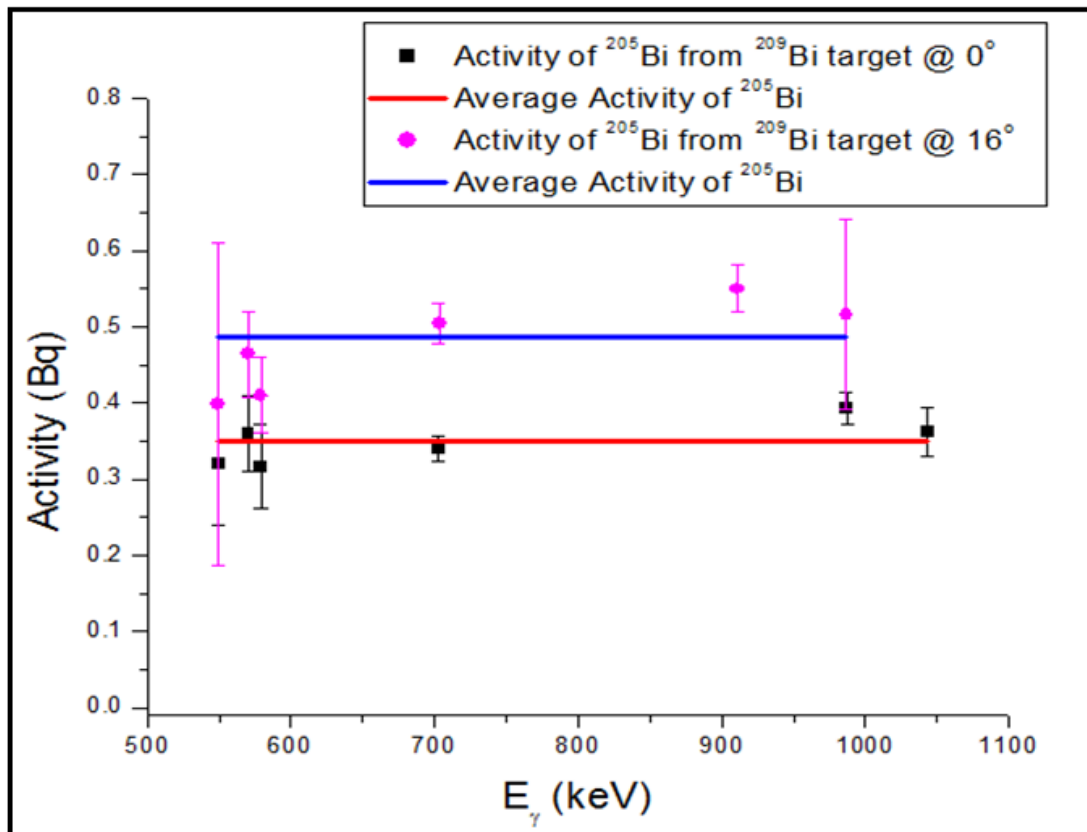


Figure 4.13. The activity (Bq) of ^{205}Bi radionuclide as a function of energy for the reaction of $^{209}\text{Bi}(n,5n)$ at neutron beam energy of 140 MeV.

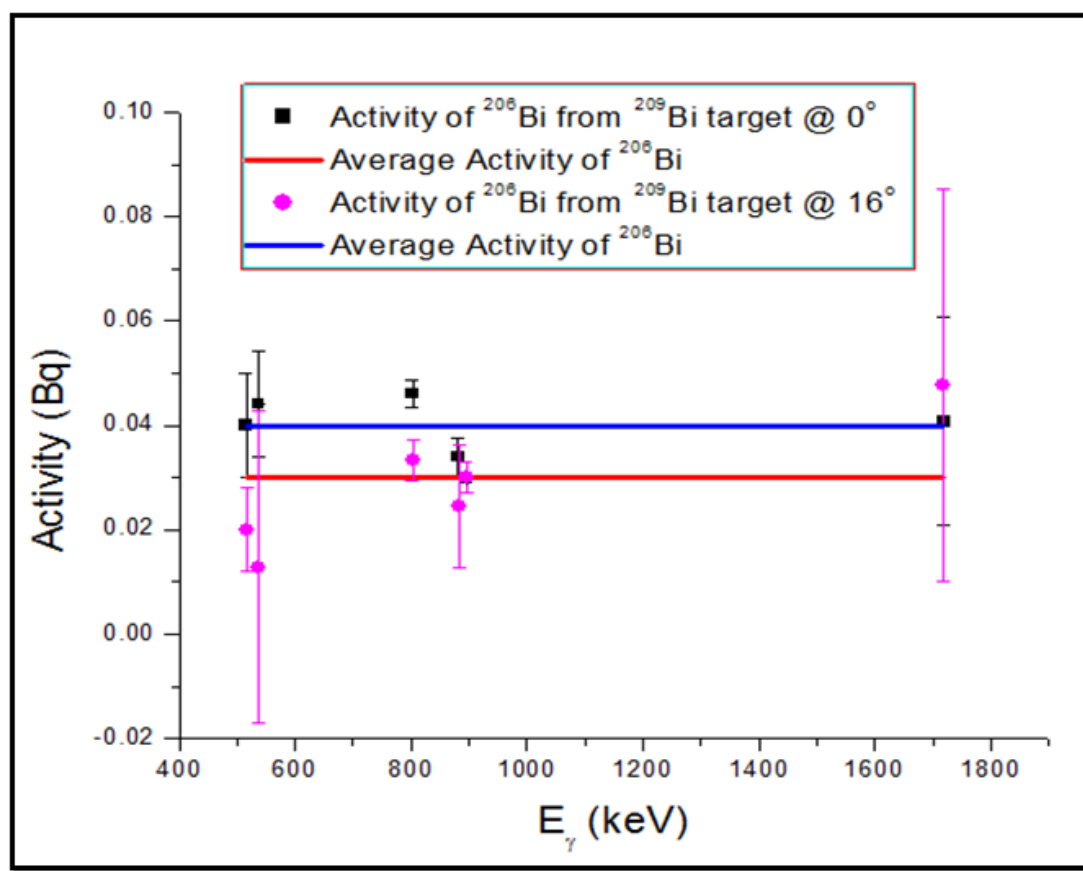


Figure 4.14. The activity (Bq) of ²⁰⁶Bi radionuclide as a function of energy for the reaction of ²⁰⁹Bi(n,4n) at neutron beam energy of 140 MeV.

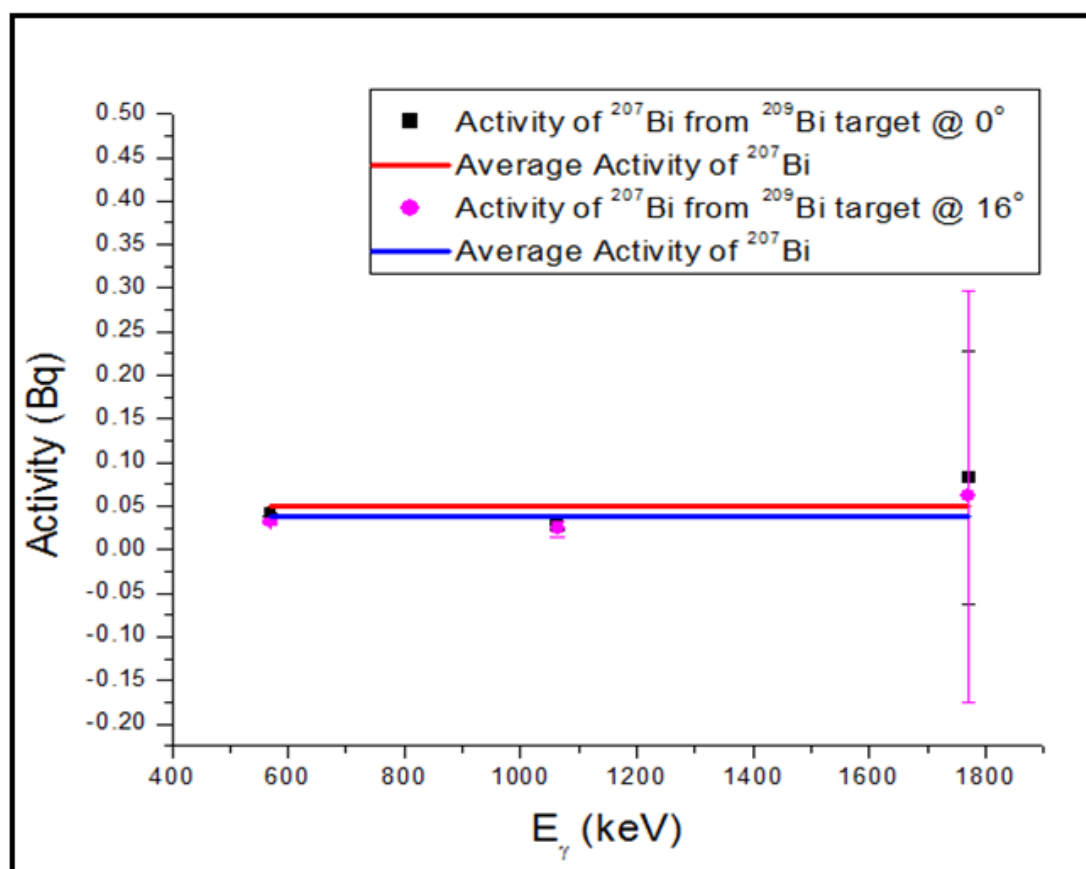


Figure 4.15. The activity (Bq) of ^{207}Bi radionuclide as a function of energy for the reaction of $^{209}\text{Bi}(n,3n)$ at neutron beam energy of 140 MeV.

After estimating the activity of each radionuclide, the next step was to determine the production cross section, but first the background (which is the irradiation due to the low energy neutron beams) was removed by subtracting the activity (A_{16°) from activity (A_{0°), $A = A_{0^\circ} - A_{16^\circ}$. Only gamma lines of energies with high intensity were used. This was for the purpose of minimizing the uncertainties that may have been caused by gamma energies with low intensity. Note also that because of large uncertainties due to neutron beam characterisations, other parameters (e.g. neutron fluence, beam fluctuators) had a negative effect on the production of some of the expected radionuclides.

4.3 Calculations of the Production Cross-section

In this study radionuclides produced from the neutron induced reaction $^{209}\text{Bi}(\text{n},\text{xn})$ are ^{205}Bi (15.31 days), ^{206}Bi (6.243 days) and ^{207}Bi (31.55 yrs), the aim was to produce and study all the radionuclides from $^{209}\text{Bi}(\text{n},\text{3-8n})$ reactions. However due to other nuclides being short lived (hours half life) they decayed early even before the sample was taken to HPGe detector for gamma ray counting. For that reason only (^{205}Bi , ^{206}Bi and ^{207}Bi) were identified from gamma ray spectra.

In determining the reaction cross section for the above identified nuclides, the activity corresponding to the gamma ray energy of high branching ratio was used. Equation 4.3 was used to calculate the activity of radionuclide.

$$A(t_{irr}, t_d, t_c) = N_0 \sigma \phi (1 - e^{-\lambda t_{irr}}) e^{-\lambda t_d} (1 - e^{-\lambda t_c}) \quad (4.3)$$

where $A(t_{irr}, t_d, t_c)$ = is the activity of a radioactive nucleus during the gamma ray measurement, N_0 = is the number of target nuclei, σ = is the cross section (cm^2), ϕ = is the neutron flux, λ = is the decay constant in s^{-1} , t_{irr} = is irradiation time, t_d = is delayed time and t_c = is counting time. Equation 4.4 was used to calculate the reaction cross section, and it was derived from the activity in Equation 4.3 above. The uncertainty of the cross section was estimated using the error propagation rule on Equation 4.5, where A_{error} is the error of the activity and ϕ_{error} is the error of neutron flux.

$$\sigma = \frac{A}{N_0 \phi (1 - e^{-\lambda t_{irr}}) e^{-\lambda t_d} (1 - e^{-\lambda t_c})} \quad (4.4)$$

$$\sigma_{error} = \sigma * \sqrt{\left(\frac{A_{error}}{A}\right)^2 + \left(\frac{\phi_{error}}{\phi}\right)^2} \quad (4.5)$$

The results found after calculating the cross section are presented in a Table 4.3.

Table 4.3. Table that shows the cross section result of neutron induced reactions.

Neutron energy (MeV)	Target	Reactions	Gamma ray energy (keV)	Activity (Bq) $A = A_{0^\circ} - A_{16^\circ}$	reaction cross section (b)
90	^{209}Bi	$^{209}\text{Bi}(n,5n)^{205}\text{Bi}$	703.44 (0.31)	4.79 ± 0.24	0.1118 ± 0.0056
		$^{209}\text{Bi}(n,4n)^{206}\text{Bi}$	803.10 (0.99)	1.63 ± 0.08	0.0959 ± 0.0048
		$^{209}\text{Bi}(n,3n)^{207}\text{Bi}$	569.70 (0.9774)	0.17 ± 0.01	0.0066 ± 0.0005
140	^{209}Bi	$^{209}\text{Bi}(n,5n)^{205}\text{Bi}$	703.44 (0.31)	0.1652 ± 0.0099	0.0131 ± 0.0008
		$^{209}\text{Bi}(n,4n)^{206}\text{Bi}$	803.10 (0.99)	0.0126 ± 0.0013	0.0065 ± 0.0007
		$^{209}\text{Bi}(n,3n)^{207}\text{Bi}$	569.70 (0.9774)	0.0094 ± 0.0008	0.00088 ± 0.000075

The results from Table 4.3 are presented in the next section in a form of the plots, and they are also compared with the previously measured and evaluated data. A_{0° is the activity of radionuclide that was produced from target which was irradiated using high energy (quasi-monoenergetic) neutron beams. A_{16° is the activity of radionuclide that was produced from target which was irradiated using low energy (continuum tail) neutron beams and A is the background corrected activity.

Due to the delay in finalising the neutron spectra from the monitors, neutron flux value of $4 \times 10^4 \text{ cm}^{-2} \cdot \text{s}^{-1}$ was used as previously used by Nolte (2002) [37]. In their study, the same neutron beam facility of iThemba LABS was used. Moreover, the total error estimate in the final cross section was affected mainly by the following components summarized in Table 4.4, 7% due to the error estimate in the measurements of peak fluences, 4% peak to continuum ratio, 2% fluence monitor, 4% for HPGe detection efficiency and 5-30% counting statistics [6, 37].

Table 4.4. Table shows the components that contribute to the uncertainty of the production cross section of radionuclides.

Components	iTL data (by Sisterson (2005) [6] and Nolte (2002) [37])	Kim (1999 [40])
Peak fluence	7 %	3.4 - 15 %
Monitoring	2 %	-
Efficiency (Ge)	4 %	4 %
Counting stats	< 2 %	0.4 - 43 %

4.3.1 $^{209}\text{Bi}(n,5n)^{205}\text{Bi}$ reaction

^{205}Bi is one of the long lived radionuclides produced from the $^{209}\text{Bi}(n,5n)^{205}\text{Bi}$ reaction using quasi-monoenergetic neutron beams of 90 and 140 MeV energy. The radionuclide ^{205}Bi decayed to ^{205}Pb by and electron process capture (100%). The ^{205}Bi was identified by its two intense γ -lines of 703.44 keV ($I_\gamma = 31\%$) and 987.62 keV ($I_\gamma = 16.13\%$) [38]. The $^{209}\text{Bi}(n,5n)^{205}\text{Bi}$ reaction cross sections from this work are given in Table 4.3. Experimental results were obtained from two neutron energies (90 and 140 MeV). The measured reaction cross sections along with the literature data and those from model calculations are shown in Figure 4.16.

The present experimental data for $^{209}\text{Bi}(n,5n)^{205}\text{Bi}$ reaction were compared with the model predictions (EAF-2010 [41]), and literature data by (Kim-1998 [42], Bhatia-2012 [43] and Vrzalova-2013 [44]).

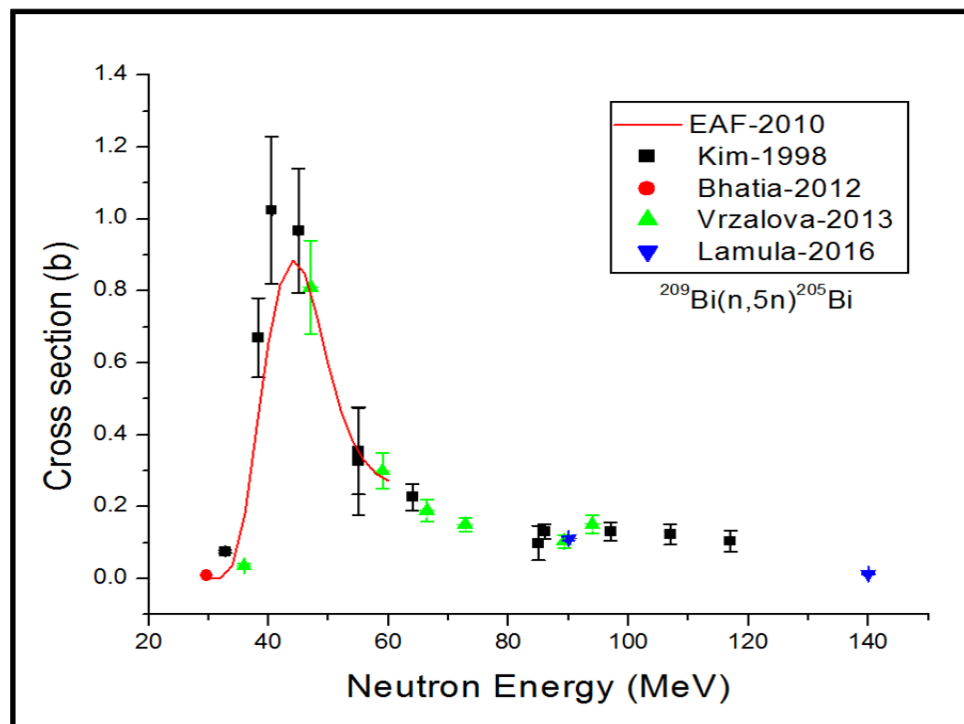


Figure 4.16. The neutron induced cross sections of $^{209}\text{Bi}(n,5n)^{205}\text{Bi}$ reaction from the present work (Lamula-2016) compared with the results of earlier measurements and model calculations.

4.3.2 $^{209}\text{Bi}(n,4n)^{206}\text{Bi}$ reaction

^{206}Bi is a radionuclide which was produced from the $^{209}\text{Bi}(n,4n)^{206}\text{Bi}$ neutron induced reaction at beam energies of 90 and 140 MeV. The nucleus ^{206}Bi decays to ^{206}Pb by electron capture process (100%) and emitted gamma rays. The ^{206}Bi was identified by its three intense γ -lines of 516.18 keV ($I_\gamma = 40.7\%$), 803.10 keV ($I_\gamma = 99.0\%$) and 881.01 keV ($I_\gamma = 66.2\%$) [38]. The $^{209}\text{Bi}(n,4n)^{206}\text{Bi}$ reaction cross sections from this present work are given in Table 4.3. Experimental results were obtained from two neutron beam energies (90 and 140 MeV). The measured reaction cross sections from this study, literature data and model calculations are shown in Figure 4.17.

The measured cross section data for $^{209}\text{Bi}(n,4n)^{206}\text{Bi}$ reaction was compared with the model predictions (TENDL-2009 [45] and EAF-2007 [46]), and literature data by (Vrzalova-2010 [44], Uddin-2009 [47], Kim-1998 [42] and Bhatia-2012 [43]).

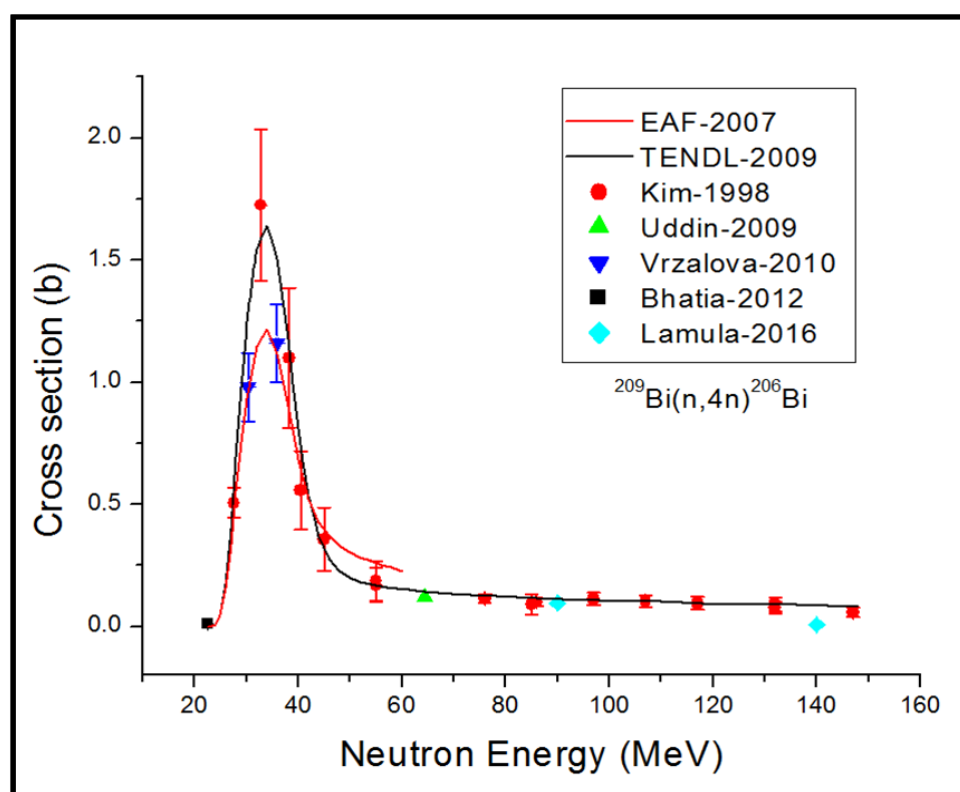


Figure 4.17. The neutron induced cross sections of $^{209}\text{Bi}(n,4n)^{206}\text{Bi}$ reaction from the present work (Lamula-2016) compared with the results of earlier measurements and model calculations.

4.3.3 $^{209}\text{Bi}(n,3n)^{207}\text{Bi}$ reaction

^{207}Bi radionuclide was produced from the $^{209}\text{Bi}(n,3n)^{207}\text{Bi}$ neutron induced reaction at beam energies of 90 and 140 MeV. The nucleus ^{207}Bi decayed to ^{207}Pb by an electron capture process (100%) and emitted gamma rays. The ^{207}Bi was identified by its γ -lines of 569.702 keV ($I_\gamma = 97.74\%$) and 1063.662 keV ($I_\gamma = 74.5\%$) [38]. The $^{209}\text{Bi}(n,3n)^{207}\text{Bi}$ reaction cross sections from this work are given in Table 4.3. Experimental results were obtained from two neutron beam energies (90 and 140 MeV). The measured reaction cross sections from this study, literature data and model calculations are shown in Figure 4.18. The measured cross section data for $^{209}\text{Bi}(n,3n)^{207}\text{Bi}$ reaction was also compared with the model predictions (EAF-2010 [41] and IRDFF-1 [48]), and literature data by (Prokopets-1980, Vrzalova-2010 [44], Kim-1998 [42] and Vesser-1976).

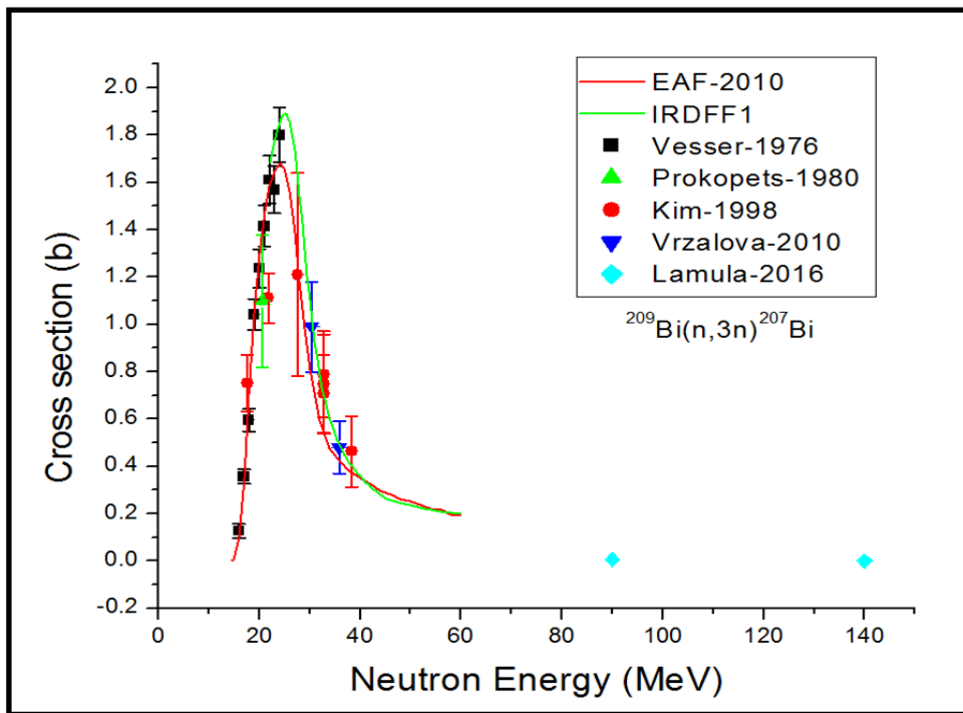


Figure 4.18. The neutron induced cross sections of $^{209}\text{Bi}(n,3n)^{207}\text{Bi}$ reaction from the present work (Lamula-2016) compared with the results of earlier measurements and model calculations.

Chapter 5

Conclusions and Recommendations

5.1 Conclusions

In this study the cross section and uncertainties for $^{209}\text{Bi}(n,xn)$ reactions were measured by the neutron activation method using quasi-monoenergetic neutron beams of 90 and 140 MeV produced by $^7\text{Li}(p,n)^7\text{Be}$ reaction. The aim was to study all $^{209}\text{Bi}(n,3-8n)$ reactions. However, the radionuclides from $^{209}\text{Bi}(n,6-8n)$ reactions are short lived and they decayed before gamma ray measurements, therefore only radionuclides from $^{209}\text{Bi}(n,3-5n)$ reactions were studied. These cross section measurements were conducted for the purpose of improving and extending the IRDFF (International Reactor Dosimetry and Fusion File) library since the available experiment data for these reactions at high neutron energies are insufficient (above 20 MeV). The measured values were compared with the available evaluated data from (TENDL, EAF and IRDFF) libraries as well as cross section data from previous measurements (Kim, Vrzalova, Uddin, Bhatia, Prokopets and Vesser) and they were found to be in a relative good agreement considering the assumptions made regarding the neutron flux and uncertainties. More analysis is underway to independently finalise the correct neutron spectra for the given irradiations and subsequently determining the correct neutron fluxes. In addition this will also assist in assigning the correct uncertainty component for each of the contribution.

The experimental results of the present work will be useful as benchmark values to evaluate nuclear data and investigate the accuracy of calculation codes. It can also help in

the adjustment of statistical model parameters to understand these reactions in terms of statistical models and for a better evaluation of these reaction cross sections in the future.

5.2 Recommendations

More gamma-ray detectors are required to also measure the short lived radionuclides. Stable beam with high neutron flux is important to improve the production rates of nuclides. In addition, the results of this study also depends on the correct and efficient way to determine correct neutron spectra and fluxes, of which are still outstanding.

Bibliography

- [1] Eismont V.P. et al. Measurements of nucleon-induced fission cross-sections of separated tungsten isotopes and natural tungsten in the 50-200 MeV energy region. 2005.
- [2] Koning A.J. et al. Nuclear data for sustainable nuclear energy. Technical report, Coordinated action on nuclear data for industrial development in Europe (CANDIDE), 2009.
- [3] Zolotarev K.I. Evaluation of cross-section data from threshold to 40 MeV for some neutron reactions important for fusion dosimetry applications. *INDC International Nuclear Data Committee*, INDC(NDS), November 2010.
- [4] Simakov S. Testing and Improving the International Reactor Dosimetry and Fusion File (IRDF). Technical report, IAEA, 2015.
- [5] Domula A.R. et al. New nuclear structure and decay results in the ^{76}Ge - ^{76}As system. *Nuclear Data Sheets*, 120:44–47, 2014.
- [6] Sisterson J.M. et al. Cross-section Measurements for Neutron-induced Reactions in Copper at Neutron Energies of 70.7 and 110.8 MeV. *Nuclear Instruments and Methods in Physics Research B*, 240(3):617–624, 2005.
- [7] Krane K.S. *Introductory Nuclear Physics*. John Wiley & Sons, Second edition, 1955.
- [8] L'Annunziata F. *Radioactivity Introduction and History*. Prof. Dr. Werner Burkart, first edition, February 2007.
- [9] Knoll G.F. *Radiation Detection and Measurements*. John Wiley & Sons, Third edition, 1999.

-
- [10] Murty K.L and Charit I. *Overview of Nuclear Reactor Systems and Fundamentals*. Wiley-VCH Verlag GmbH & Co. KGaA, first edition, 2013.
- [11] Berlizov A. *Presentation on Neutron Activation Analysis*. Institute for Nuclear Research, 8th edition, September 2006.
- [12] Zaliznyak I.A and Lee S. *Magnetic Neutron Scattering and Recent Developments in the Triple Axis Spectroscopy*. 2005.
- [13] Rinard P. *Neutron Interactions with Matter*. 2004.
- [14] Weston M. S. *Nuclear Reactor Physics*. John Wiley & Sons, Inc., Canada, 2001.
- [15] Murray R.L. and Holbert K.E. *Nuclear Energy: an introduction to the concepts, systems, and applications of nuclear processes*. Elsevier, 2015.
- [16] Elmer E.L. *Fundamentals of Nuclear Reactor Physics*. Journal of Applied Physics, 2008.
- [17] OECD-NEA. *JANIS 4.0 USERS GUIDE*. Nuclear Energy Agency, 2013.
- [18] Training Centre. *Fundamentals of Power Reactors Module One Science & Engineering Fundamentals*. Atomic Energy Control Board of Canada, 1993.
- [19] Bode P. *Instrumental and Organizational Aspects of a Neutron Activation Analysis Laboratory*. PhD thesis, Delft University of Technology, The Netherlands, December 1996.
- [20] Frontasyeva M.V. *Neutron Activation Analysis for the Life Sciences and Material Sciences*. July 2011.
- [21] Hamidatou L. et al. *Concepts, Instrumentation and Techniques of Neutron Activation Analysis*. INTECH, 2013.
- [22] Chan Y.F. *Neutron Activation Measurements for Materials Used in Fusion Reactors*. Master's thesis, University of York, September 2012.
- [23] Gerward L. *Paul Villard and his Discovery of Gamma Rays*. *Physics in Perspective*, 1:367–383, 1999.

-
- [24] Thidimu A. M. Gamma Rays. April 2003.
- [25] Henriksen T. *Radioactivity and X-rays Applications and health effects*. 2009.
- [26] Lilley J. *Nuclear Physics Principles and Application*. John Wiley & Sons, 2001.
- [27] Maleka P.P. *In-situ Element Analysis from Gamma-Ray And Neutron Spectra Using a Pulsed-Neutron Source*. PhD thesis, University of Groningen, The Netherlands, 2010.
- [28] AN34 Experiment 3. Gamma-ray spectroscopy using NaI(Tl). *EG & E ORTEC*, 1984.
- [29] Rittersdorf I. Gamma Ray Spectroscopy. Technical report, University of Michigan, USA, 2007.
- [30] Park C.S. et al. Determination of Single Escape and Double Escape Peak Efficiency for a HPGe Detector. *Journal of the Korean Nuclear Society*, 35(6):532–528, December 2003.
- [31] Reguigui N. Gamma Ray Spectrometry. September 2006.
- [32] Hastings A., Smith J., and Marcia L. Gamma-Ray Detectors. 2013.
- [33] Canberra. Gamma and X-Ray Detection. *Canberra Industries, Inc.*, 2014.
- [34] Armstrong A. and Bala I. Resolution and Efficiency of High Purity Germanium Detector. 2008.
- [35] Peetermans S. Neutron Activation Analysis. 2009.
- [36] Win D.T. Neutron Activation Analysis (NAA). (1):8–14, July 2004.
- [37] Nolte R. et al. High-energy neutron reference fields for the calibration of detectors used in neutron spectrometry. *Nuclear Instruments and Methods in Physics Research A*, 476:369–373, 2002.
- [38] Firestone R.B. *Table of Isotopes*. John Wiley & Sons, eighth edition, March 1996.
- [39] Department: Minerals and Energy Republic of South Africa. UNDERSTANDING RADIOACTIVITY & RADIATION IN EVERYDAY LIFE, APRIL 2005.

- [40] Kim E.J et al. Measurements of Activation Cross Sections on Spallation Reactions for ^{59}Co and $^{\text{nat}}\text{Cu}$ at Incident Neutron Energies of 40 to 120 MeV. *Nuclear Science and Technology*, 36(1):29–40, January 1999.
- [41] Sublet J.C et al. The European Activation File: EAF-2010 neutron-induced cross section library. *EASY Documentation Series CCFE-R*, 5, April 2010.
- [42] Kim E. et al. Measurements of Neutron Spallation Cross Sections of ^{12}C and ^{209}Bi in the 20- to 150-MeV Energy Range. *Nuclear Science and Engineering*, 129(3):209–223, July 1998.
- [43] Bhatia C. et al. A study of non-elastic reaction rates for the ADS materials in the environment of spallation neutrons produced by 1.6 GeV d-beam. *Appl. Radiat. Isot.*, 7(70):1254–60, July 2012.
- [44] Vrzalova J. et al. Studies of (n,xn) cross-sections in Al, Au, Bi, Cu, Fe, I, In, Mg, Ni, Ta, Y, and Zn by the activation method. *Nuclear Instruments and Methods in Physics Research A*, 726:84–90, 2013.
- [45] D. Rochman and A.J. Koning. Towards completeness and accuracy, November 2009.
- [46] Forrest R. A. et al. The European Activation File: EAF-2007 neutron-induced cross section library. *UKAEA Fusion Working in Europe*, March 2007.
- [47] Uddin M.S. et al. Measurements of neutron induced activation of concrete at 64.5 MeV. *Annals of Nuclear Energy*, 36(8):1133–1137, August 2009.
- [48] Zsolnay E.M. et al. Summary description of the new International Reactor Dosimetry and Fusion File (IRDFF release 1.0). *INDC International Nuclear Data Committee*, May 2012.
- [49]